

MICROCOPY RESOLUTION TEST CHART
NATIONAL BUREAU OF STANDARDS 1963 A







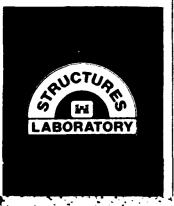
US Army Corps of Engineers











RESPONSE OF EARTH-COVERED SLABS IN CLAY AND SAND BACKFILLS

S. A. Kiger, P. S. Eagles, and J. T. Baylot

Structures Laboratory

DEPARTMENT OF THE ARMY Waterways Experiment Station. Corps of Engineers PO Box 631 Vicksburg, Mississippi 39180-0631





В

October 1984 Final Report

Approved For Public Release, Distribution Unlimited

OTIC FILE COPY

Prepared for Defense Nuclear Agency Washington, DC 20305

and DEPARTMENT OF THE ARMY US Army Corps of Engineers Washington, DC 20314-1000

DNA Subtask Y99QAXSC062, Work Unit 42. DNA Subtask H19IAXSX337, Work Unit 02, and OCE R&D Project 4A762719AT40, Task A0. Work Unit 008

Destroy this report when no longer needed. Do not return it to the originator.

The findings in this report are not to be construed as an official Department of the Army position unless so designated by other authorized documents.

The contents of this report are not to be used for advertising, publication, or promotional purposes. Citation of trade names does not constitute an official endorsement or approval of the use of such commercial products.

SECURITY CLASSIFICATION OF THIS PAGE (When Date Entered)

REPORT DOCUMENTATION PAGE	READ INSTRUCTIONS BEFORE COMPLETING FORM					
T. REPORT NUMBER	3. RECIPIENT'S CATALOG NUMBER					
Technical Report SL-84-18 AD-714	276					
4. TITLE (and Subtitle)	5. TYPE OF REPORT & PERIOD COVERED					
RESPONSE OF EARTH-COVERED SLABS IN CLAY	Final report					
AND SAND BACKFILLS	6. PERFORMING ORG. REPORT NUMBER					
7. AUTHOR(a)	8. CONTRACT OR GRANT NUMBER(#)					
S. A. Kiger P. S. Eagles						
J. T. Baylot						
9. PERFORMING ORGANIZATION NAME AND ADDRESS	10. PROGRAM ELEMENT, PROJECT, TASK AREA & WORK UNIT NUMBERS					
US Army Engineer Waterways Experiment Station						
Structures Laboratory PO Poy 621 Violeburg Mississippi 20180 0621	See Block 18					
PO Box 631, Vicksburg, Mississippi 39180-0631	12. REPORT DATE					
Defense Nuclear Agency, Washington, DC 20305;	October 1984					
and DEPARTMENT OF THE ARMY, US Army Corps of	13. NUMBER OF PAGES					
Engineers, Washington, DC 20314-1000 14. MONITORING AGENCY NAME & ADDRESS(If different from Controlling Office)	72 15. SECURITY CLASS. (of this report)					
14. MONITORING AGENCY NAME & ADDRESSIT GREETER TOUR COMMONING COMMONING	is. secont i censs (s. me repair)					
	Unclassified					
	15a. DECLASSIFICATION DOWNGRADING SCHEDULE					
16. DISTRIBUTION STATEMENT (of this Report)						
TO DISTRIBUTION STATEMENT (STATE TOPOLT)						
Approved for public release; distribution unlimited.						
17. DISTRIBUTION STATEMENT (of the abstract entered in Block 20, If different from Report)						
THE STATE OF THE SMELL COLUMN STATES OF THE						
18. SUPPLEMENTARY NOTES						
Available from National Technical Information Serv	ice, 5285 Port Royal Road,					
Springfield, Virginia 22161.						
Prepared Under DNA Subtask Y99QAXSC062, Work Unit						
Work Unit 02, and OCE R&D Project 4A762719AT40, Ta	SK AU, WORK CHIE OUG.					
Airblast simulation Hardened installat						
Compressive membrane stress Nuclear explosion	simulation Survivability					
Concrete slabs Shallow-buried str	• • • • • • • • • • • • • • • • • • • •					
Concrete structures Soil arching	structures Vulnorability					
Dynamic tests Soil-structure 11tt 20. ABSTRACT (Confinue on reverse elds if recessary and identify by block number)	eraction Yulnerability					
Five tests were conducted, three static and t						
2-foot-wide, one-way reinforced concrete slabs. E	ach slab was 2 feet long and					
had a span-to-effective-depth ratio of 10. Static tests were conducted using						
water over a waterproof membrane to apply a uniform surface pressure with the test slabs surface flush, I foot deep in a clay soil backfill, and I foot deep						
test slabs surface flush, I foot deep in a clay so in a sand backfill. The clay and sand backfill co						
the two dynamic tests.						
	(Continued)					

20. ABSTRACT (Continued).

The reaction structure supporting the slabs was rigid enough to prevent any slab support rotation at the clamped edges. The rigid reaction structure also eliminated any inplane thrust generated by lateral earth pressures. Therefore, compressive membrane thrust was not a variable between the tests.

The surface-flush static test slab failed at about 174 psi, failure in the static clay backfill test occurred at about 174 psi, and failure in the static sand backfill test occurred at about 835-psi overpressure. The approximately fivefold increase in static capacity in the sand backfill was due to soil arching in the high-shear-strength sand backfill.

Peak dynamic pressure in the dynamic sand backfill test was approximately 3,300 psi and in the dynamic clay backfill test about 860 psi. \ Interface pressure data indicate soil arching also occurred in the dynamic tests. In the sand backfill test, less impulse was recorded over the flexible center of the slab than was recorded over the slab support. Dynamic soil arching was much less in the clay backfill.

These test results indicate that soil arching, both static and dynamic, is much more important than current calculations indicate at this very shallow burial depth.

The dynamic tests approximately simulated 0.027- and 0.010-KT nuclear weapons at about 3,300- and 860-psi peak overpressures, respectively. Assuming a 16-foot prototype span, these weapons scale up to approximately 14 and 5 KT, respectively.

Unclassified

PREFACE

Research reported herein was sponsored by the Defense Nuclear Agency (DNA) under Subtask Y99QAXSC062, Work Unit 42, "Shallow-Buried Structures," and by the Office, Chief of Engineers, U. S. Army, under R&D Project 4A76219AT40, Task AO, Work Unit 008, "Target Response from Low-Yield Nuclear Surface and Subsurface Bursts." The backfill material property and geophysical work was conducted for DNA under Subtask H19IAXSX337, Work Unit 02, "Buried Structures." Dr. K. L. Goering, DNA, was Technical Monitor.

Construction and testing were conducted by personnel of the Structures Laboratory (SL), U. S. Army Engineer Waterways Experiment Station (WES), under the general supervision of Mr. Bryant Mather, Chief, SL, and Mr. James T. Ballard, Assistant Chief, SL, and under the direct supervision of Dr. Jimmy P. Balsara, Acting Chief, Structural Mechanics Division (SMD), SL. This report was prepared by Dr. S. A. Kiger, and Messrs. P. S. Eagles and J. T. Baylot of the Research Group, SMD.

COL Tilford C. Creel was Commander and Director of WES during the preparation of this report. Mr. F. R. Brown was Technical Director.

Accession For	/
NIIS CEASI	
PTTO TO	7 1 1 1 1 1 1 1 1 1 1 1 1 1 1 1 1 1 1 1
Unit of the A	1
J. 5 . 5 . 5 . 5 .	
l By	-
ptyle Troten/	
1	Codes
10 1 1 1 1 1 1 1 1 1 1 1 1 1 1 1 1 1 1	
Dist	_
A 1	
A-I	



CONTENTS

	Page
PREFACE	1
LIST OF ILLUSTRATIONS	3
LIST OF TABLES	4
CONVERSION FACTORS, NON-SI TO SI (METRIC) UNITS OF MEASUREMENT	5
CHAPTER 1 INTRODUCTION	6
1.1 BACKGROUND	6
1.2 OBJECTIVE	6 6
CHAPTER 2 STRUCTURAL DETAILS AND MATERIAL PROPERTIES	8
	8
2.1 CONCRETE	8
2.3 REID-BEDFORD SAND	8
2.4 CLAY BACKFILL	9
CHAPTER 3 EXPERIMENTAL PROCEDURE	14
3.1 TEST FACILITY FOR STATIC TESTS	14 14
3.3 INSTRUMENTATION PLAN FOR STATIC TESTS	15
3.4 TEST FACILITY FOR DYNAMIC TESTS	15
3.5 TEST PLAN FOR DYNAMIC TESTS	15 16
CHAPTER 4 TEST RESULTS	22
4.1 DATA	22
4.2 STATIC TEST DATA	22
4.2.1 Surface-Flush Static Test (Test 1)	23
4.2.2 Static Test in Sand (Test 2)	23 25
4.2.3 Static Test in Clay (Test 3)	25 25
4.3.1 Dynamic Test in Sand (Test 4)	26
4.3.2 Dynamic Test in Clay (Test 5)	27
CHAPTER 5 ANALYSIS	57
5.1 MAXIMUM RESISTANCE	57
5.2 SOIL ARCHING	59
5.3 WEAPON SIMULATION	61
5.4 DYNAMIC RESPONSE	61
CHAPTER 6 CONCLUSIONS	67
REFERENCES	68

LIST OF ILLUSTRATIONS

Figure		Page
2.1	Reinforcement details and dimensions	. 12
2.2	Shear reinforcement details	. 13
3.1	6,000-psi static test chamber	. 17
3.2	Reaction structure	
3.3	Instrumentation for Static Test 1	. 18
3.4	Instrumentation for Static Test 2	. 19
3.5	Instrumentation for Static Test 3	. 19
3.6	Foam HEST configuration	. 20
3.7	Foam HEST charge cavity, Tests 4 and 5	. 20
3.8	Instrumentation for Tests 4 and 5	. 21
4.1	Initial loading of surface-flush static test	
4.2	Surface-flush static test slab following initial	,
	loading	. 29
4.3	Ultimate capacity of surface-flush slab	
4.4	Collapse loading of surface-flush slab	
4.5	Failure of surface-flush static test slab	. 31
4.6	Resistance for sand-backfill static test	
4.7	Centerline interface pressure in sand-backfill test	
4.8	Quarter-point interface pressure in sand-backfill test	
4.9	Interface pressure at end of clear span in sand-	. 33
4.7	backfill test	. 33
4.10	Centerline soil stress in sand-backfill test	
4.11	Quarter-point soil stress in sand-backfill test	
4.12	Soil stress near end of clear span in sand-backfill test	
4.13	Soil stress over support in sand-backfill test	
4.14	Posttest photograph of the sand-backfill static test slab	
4.15	Resistance in static clay-backfill test	_
4.16	Centerline interface pressure in static clay-backfill test	
4.17	Quarter-point interface pressure in static clay-	. 57
4.17	backfill test	. 38
4.18	Interface pressure near support in static clay-	. 50
4.10	backfill test	. 38
4.19	Soil stress over slab support in static clay-backfill test	
4.20	Posttest photograph of slab in static clay-backfill test	
4.21	Dynamic overpressure record in Test 4	
4.22	Airblast pressure from Test 4 and weapon simulation	
4.23	Posttest view of Test 4 slab failure	
4.24		
4.25	Closeup view of Test 4 slab	
4.25	Interface pressure 7 inches from the center of the	. 43
4.20	slab in Test 4	. 43
4.27	Interface pressure 11 inches from the center of the	. 43
4.21	slab in Test 4	. 44
4.28	Free-field soil stress in Test 4	
4.20	Soil stress over the slab support in Test 4	
4.29	Centerline deflection of slab in Test 4	
4.30	Airblast pressure from Test 5 measured by BP1	
4.31	Airblast pressure from Test 5 measured by BP3	
4.32	Pressure-time records and simulation, Test 5	
4.JJ	rressure-rime records and simuration, rest 1	. 40

<u>Figure</u>		Page					
4.34	Impulse-time records and simulation, Test 5	48					
4.35	Alternate Test 5 simulation	49					
4.36	Posttest photographs of Test 5 slab	50					
4.37	Test 5 deflection record	51					
4.38	IF1 interface data from Test 5	52					
4.39	IF2 interface data from Test 5	53					
4.40	IF3 interface data from Test 5	54					
4.41	SE1 soil stress data from Test 5	55					
4.42	SE2 soil stress data from Test 5	56					
5.1	Soil-arching ratio	63					
5.2	Dynamic load factors, BP1, Test 4, 10-ms record	64					
5.3	Dynamic load factors, BP3, Test 5, 10-ms record	65					
5.4	Dynamic load factors, BP3, Test 5, 2-ms record	66					
LIST OF TABLES							
Table 2.1	Concrete compressive strength and modulus of elasticity,						
	day of test	10					
	Static tensile test, steel wire reinforcement	11					

•

CONVERSION FACTORS, NON-SI TO SI (METRIC) UNITS OF MEASUREMENT

Non-SI units of measurement used in this report can be converted to SI (metric) units as follows:

Multiply	Ву	To Obtain
degrees (angle)	0.01745	radians
feet	0.3048	metres
grains per foot	0.212594849	grains per metre
inches	2.54	centimetres
inches per second	0.0254	metres per second
kilotons	4.184	megajoules
pounds (force)	4.448222	newtons
pounds (force) per inch	0.1751268	kilonewtons per metre
pounds (force) per square inch	6.894757	kilopascals
pounds (mass) per cubic foot	16.01846	metre
tons (force) per square foot	95.76052	kilopascals
<pre>pounds (force) per square inch- second</pre>	6.894	kilopascal-seconds
square inches	6.4516	square centimetres

RESPONSE OF EARTH-COVERED SLABS IN CLAY AND SAND BACKFILLS

CHAPTER 1

INTRODUCTION

1.1 BACKGROUND

Test results from the Shallow-Buried Structures (SBS) Research Program at the U. S. Army Engineer Waterways Experiment Station (WES) (References 1-7) indicate that a relatively shallow earth cover over a flat-roofed structure can significantly decrease structural response in a high-overpressure environment. Data indicate that a pressure redistribution produced by a system of shear stresses in the soil is responsible for most of the increased structural hardness. This phenomenon is generally referred to as "soil arching" and can occur in both static and dynamic load cases. Soil arching is defined as the transfer of loads from one location to another, through a system of shear stresses, in response to relative displacements within the soil. Soil arching has been studied in some detail, at least in the static case, and experimental data are reported in References 1-12. However, except for the SBS research, most of the static experiments were conducted on relatively small models, and prior to the SBS research there were almost no data on dynamic soil arching. The mitigating effects of soil arching are generally ignored in the design of shallow-buried protective structures, and this approach can result in costly, overly conservative designs. It would be equally misleading to ignore soilarching effects in a targeting calculation.

1.2 OBJECTIVE

The objective of this study was to evaluate the effects of soil cover on the static and dynamic capacity of earth-covered reinforced concrete slabs.

1.3 SCOPE

Five tests were conducted in this study, three static and two dynamic. Every effort was made to vary only one parameter, backfill type, between tests. All test slabs were made from the same concrete pour. They were 2 feet 1 square with 1-percent total principal reinforcement. The reaction structure was designed to eliminate in-plane thrust loads from lateral earth pressures which vary with backfill type. Two backfill types were used, a low-shear-strength clay and a high-shear-strength sand. Static tests were conducted on one slab flush with the surface to serve as a baseline, and on two slabs buried 1 foot deep. One was buried in clay and the other was buried in sand. The two dynamic tests repeated the clay and sand backfill conditions. Weapons simulated in the dynamic tests were approximately 0.027 and 0.010 KT which, assuming a prototype span of 16 feet, scale up to approximately 14 and 5 KT, respectively. Peak pressures in the dynamic tests were about 3,300 and 860 psi, respectively.

A table of factors for converting from non-SI to SI (metric) units of measure can be found on page 5.

CHAPTER 2

STRUCTURAL DETAILS AND MATERIAL PROPERTIES

The structures tested were reinforced concrete slabs with span-to-effective-depth ratios of 10. The slabs were 24 inches long, 24 inches wide, and 2.9 inches thick overall, including 0.5 inch of concrete cover on the tension steel. Principal reinforcing steel was 0.5 percent for both tension and compression and shear reinforcement was 0.25 percent. Structural details and dimensions are shown in Figure 2.1, and details of the shear reinforcement are shown in Figure 2.2.

2.1 CONCRETE

Type 1 Marquette cement was used in the concrete mixture which was designed to produce a 28-day strength of 6,000 psi for cylinders cured similarly to the structure. Three cylinders were tested to determine the 28-day strength. The strength varied from 6,050 to 6,450 psi with the average strength equal to 6,260 psi. Results of concrete cylinder tests, performed on the day of each slab test, are shown in Table 2.1.

2.2 REINFORCEMENT

All reinforcement steel was small-diameter wire. The wire was first cleaned with acid and then allowed to rust to obtain a surface roughness. The principal flexural steel was 0.177-inch-diameter deformed wire with an average yield strength of 90,200 psi. The temperature and shear steel were 0.125- and 0.08-inch-diameter wire, respectively, with average yield strengths of 97,500 and 84,300 psi, respectively. Results of static tensile tests for the reinforcing steel are given in Table 2.2.

2.3 REID-BEDFORD SAND

In all tests conducted in a sand backfill, a locally available sand called Reid-Bedford model sand, which has been used for several test programs at WES, was used. Reid-Bedford model sand is a uniform fine sand classified as SP in the Unified Soil Classification System and has a coefficient of uniformity $c_{\underline{u}}$ of 1.5. Its specific gravity, $G_{\underline{s}}$, is 2.66, and its maximum and minimum laboratory dry unit weights are 104.2 and 87.2 lb/ft 3 , respectively. Consolidated drained direct shear tests on this sand at initial dry unit weights

from 94 to 105.0 lb/ft^3 revealed that the friction angle increases from 30.0 to 36.0 degrees with increasing dry unit weight. The initial dry density for these tests was about 192 lb/ft^3 . For a thorough description of Reid-Bedford model sand, see Reference 10.

2.4 CLAY BACKFILL

Tests using a clay backfill were conducted in a locally available clay called Vicksburg buckshot clay. An analysis of the mineral content of the minus-74-micron (No. 200) fraction of this clay (Reference 8) yielded the following approximate breakdown:

Montmorillonite	25%
Illite	25%
Quartz	20%
Feldspar	20%
Fe ₂ 0 ₃	2%
Organic matter	1%

The specific gravity of the grains is about 2.70. Reference 8 also gives the following properties for clay consolidated to pressures of 8.2 tsf:

Coefficient of permeability =
$$3.94 \times 10^{-10}$$
 in/s
Coefficient of consolidation = 3.1×10^{-6} in²/s
Compression index = 0.52 ± 0.04

The clay, classified as CH in the Unified Soil Classification System, is highly plastic with a liquid limit of 64.5 percent and a plasticity index of 36.0 percent. It is described in some detail in References 8 and 9.

Table 2.1. Concrete compressive strength and modulus of elasticity, day of test.

Test No.	Sample No.	Compressive Strength f'	Modulus of Elasticity E	
		psi	10 ⁶ psi	
1	1	6,590	4.29	
1	2	6,890	4.50	
2	1	6,590	4.39	
2	2	6,950	4.50	
3	1	7,130	4.73	
3	2	6,710	4.28	
4 and 5	1	7,020	4.62	
4 and 5	2	6,840	4.50	

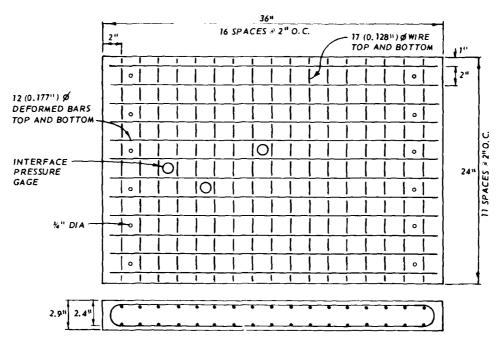
Table 2.2. Static tensile test, steel wire reinforcement.

Sample No.	Ultimate Load lb	Ultimate Stress psi	Yield Load <u>lb</u>	Yield Strength psi	Diam- eter <u>in</u>	Area in ²	Elongation for 8-in gage length %
1	2,400	97,561	2,200	89,431	0.177	0.0246	5.0
2	2,440	99,187	2,225	90,447	0.177	0.0246	4.2
3	2,440	99,187	2,210	89,837	0.177	0.0246	4.6
4	2,490	101,220	2,260	91,870	0.177	0.0246	5.4
5	2,420	98,374	2,200	89,431	0.177	0.0246	4.5
6	1,480	118,400	1,250	100,000	0.126	0.0125	3.6
7	1,490	119,200	1,220	97,600	0.126	0.0125	3.5
8	1,470	117,600	1,180	94,400	0.126	0.0125	5.0
9	1,480	118,400	1,220	97,600	0.126	0.0125	3.9
10	1,500	120,000	1,225	98,000	0.126	0.0125	3.4
11	528	105,600	435	87,000	0.080	0.0050	3.1
12	515	103,000	413	82,600	0.080	0.0050	3.4
13	512	102,400	420	84,000	0.080	0.0050	3.4
14	503	100,600	415	83,000	0.080	0.0050	2.2
15	517	103,400	425	85,000	0.080	0.0050	2.4

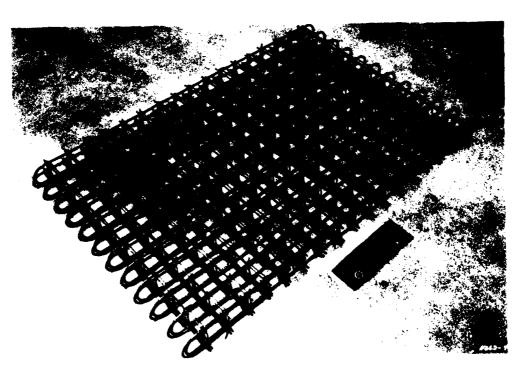
^aSamples 1-5 = main steel

^{6-10 =} temperature steel

^{11-15 =} shear steel

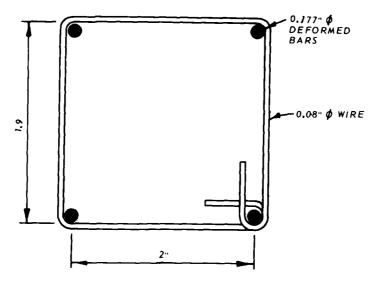


a. Reinforcement pattern

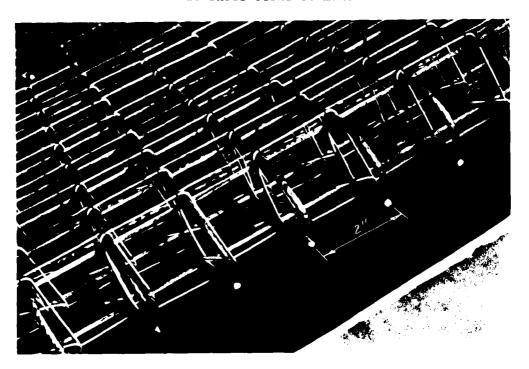


b. Reinforcement mat

Figure 2.1. Reinforcement details and dimensions.



a. Shear reinforcement



b. Shear stirrups

Figure 2.2. Shear reinforcement details.

CHAPTER 3

EXPERIMENTAL PROCEDURE

3.1 TEST FACILITY FOR STATIC TESTS

The surface-flush test was conducted in the Small Blast Load Generator (SBLG) at WES (Reference 13). The two remaining static tests (Tests 2 and 3) were run in the 6,000-psi test chamber with the reaction structure buried under 1 foot of sand for Test 2 and 1 foot of clay for Test 3.

The 6,000-psi test chamber uses the central firing station (CFS), a massive posttensioned concrete structure, as a reaction structure. The test chamber itself is a cylinder 46-3/4 inches in diameter and 40 inches high. It has a piston-type lid that seals the top and rests on a steel plate with an 0-ring to seal the bottom. A detailed drawing of this chamber is shown in Figure 3.1. When the test chamber is inside the CFS, it is sandwiched between the upper bearing block and the spacer blocks. The entire assembly of bearing block, test chamber, and spacer blocks rests on a platen which can be rolled in and out of the CFS with the assembly on it.

The SBLG can produce static pressures up to 2,000 psi. The generator has a cylindrical steel shell and an elliptical dome top. The shell is composed of a series of stacked rings of various widths, all 46-3/4 inches in inside diameter, that can be bolted together according to the depth of the sample being tested. An air-driven pump loads the test sample by means of water pressure, the water being separated from the soil-structure system by a flexible rubber diaphragm. A more complete description of these test facilities, their performance, and their calibration is given in Reference 13.

The reaction structure for the concrete slab elements was a steel box with a concrete inner lining. Six studs which were located on each end of the box were used, together with two steel plates, to clamp the elements in place. The reaction structure, used for both the static and dynamic tests, was designed to ensure one-way action of the test slabs. A photograph of the reaction structure is shown in Figure 3.2.

3.2 TEST PLAN FOR STATIC TESTS

In each test, sand was placed around the reaction structure until flush with the slab surface. Test 1 was a surface-flush test with a flexible rubber

diaphragm separating the slab, reaction structure, and sand from the pressurized water. For Test 2, 1 foot of sand was placed over the slab. A 1-foot layer of buckshot clay covered the slab for Test 3. The sand in Test 2 was vibrated to ensure uniform density. The clay in Test 3 was pounded with a mechanical "whacker." Material properties for the sand and buckshot clay are given in Chapter 2.

3.3 INSTRUMENTATION PLAN FOR STATIC TESTS

Detailed instrumentation plans are shown in Figures 3.3 through 3.5 for all three static tests. A Norwood pressure gage was mounted in the pressure chamber to measure static water pressure exerted on the soil-structure system. A Transtek Model 245-000 deflection gage, with a maximum range of 4 inches, was placed under the slab inside the reaction structure in all three static tests to measure the midspan slab deflection. Instrumentation for Static Test i is shown in Figure 3.3. For Static Tests 2 and 3, three Kulite VM 750 interface (IF) gages with a maximum range of 2,000 psi were mounted in the test slabs to measure surface stress, and soil stress (SE) gages were buried in the soil 2 inches above the slabs. The SE gages, developed at WES, are double-diaphragm gages with semiconductor sensing elements and a maximum range of 2,000 psi. Instrumentation plans for Static Tests 2 and 3 are shown in Figures 3.4 and 3.5.

3.4 TEST FACILITY FOR DYNAMIC TESTS

Both dynamic tests were conducted at the Big Black Test Site southeast of Vicksburg on the Big Black River. This facility is used by WES for various types of explosive testing.

3.5 TEST PLAN FOR DYNAMIC TESTS

Two nuclear weapon simulation tests using high explosives (HE) were conducted using pentaerythrite tetranitrate (PETN), commonly known as primacord, made into 400-gr/ft strands of detonating cord. Both tests employed a Foam HEST (High-Explosive Simulation Technique) to generate the dynamic overpressure. Figure 3.6 shows the layout of the reaction structure, charge cavity, and soil overburden for both dynamic tests. The Foam HEST used in this study can simulate the overpressure component of the airblast generated by a nuclear

detonation. This technique makes it possible to produce a uniform dynamic pressure over a large area for a sufficient duration to simulate the impulse associated with a nuclear weapon. Discussions of the foam HEST are given in References 14, 15, and 16.

In the first dynamic test (Test 4), the structure was buried in sand to a depth of 1 foot. The sand was compacted first using a hand compactor and later vibrated to ensure uniform backfill density. The 6- by 6-foot by 4.5-inch charge cavity (Figure 3.7) was then centered over the reaction structure. A charge density of $1.37 \, \text{lb/ft}^3$ was used in the cavity. Finally, a 32-inch uncompacted native soil overburden, with an approximate density of $1.0 \, \text{lb/ft}^3$, was placed over the charge cavity.

The size of the test bed, depth of burial, depth of soil overburden, and charge cavity for the second dynamic test (Test 5) were the same as for Test 4. However, the reaction structure was buried in a clay backfill and the charge density was reduced to $0.43~{\rm lb/ft}^3$.

3.6 INSTRUMENTATION PLAN FOR DYNAMIC TESTS

Detailed instrumentation plans are shown in Figure 3.8 for both dynamic tests. The Transtek Model 245~000 deflection gage used to measure midspan slab deflection in the static tests was also used for these two tests. Airblast pressure gages with four 1/4-inch-diameter baffle holes were employed to measure the airblast pressure inside the charge cavity. Three of the same Kulite VM 750 interface gages used in the static tests were used in the dynamic series. Both dynamic tests employed two SE gages placed 2 inches above the slab surface. The airblast gages were positioned at grade level inside the charge cavity.

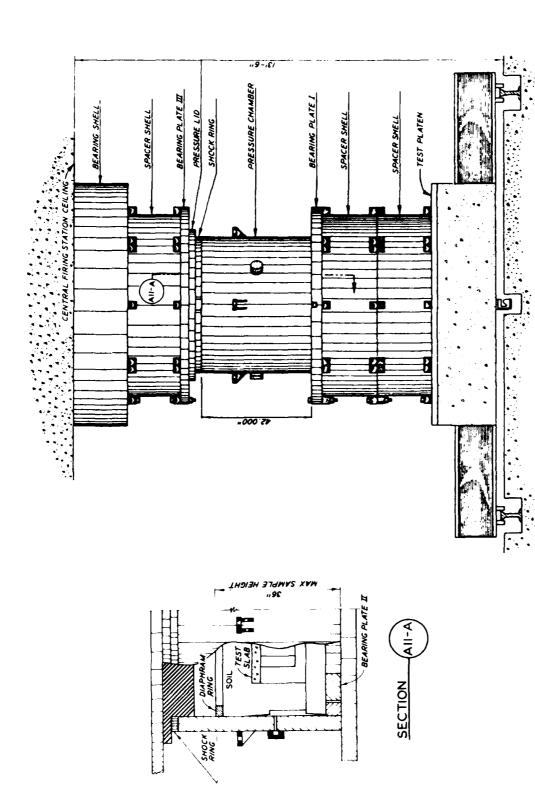


Figure 3.1. 6,000-psi static test chamber.

PRESSURE ASSEMBLY



Figure 3.2. Reaction structure.

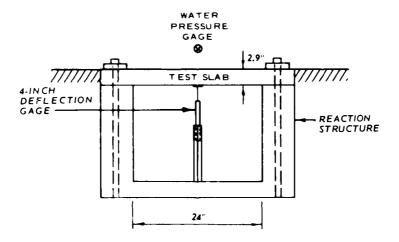


Figure 3.3. Instrumentation for Static Test 1.

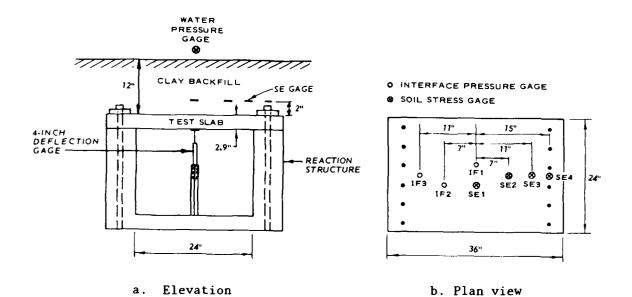


Figure 3.4. Instrumentation for Static Test 2.

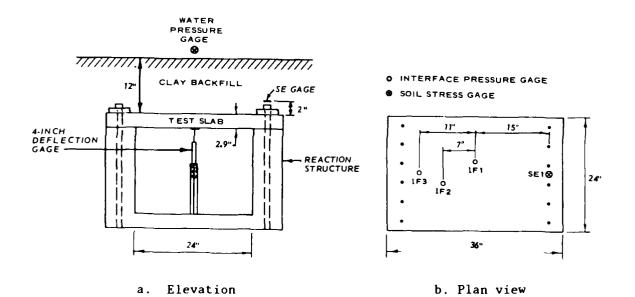


Figure 3.5. Instrumentation for Static Test 3.

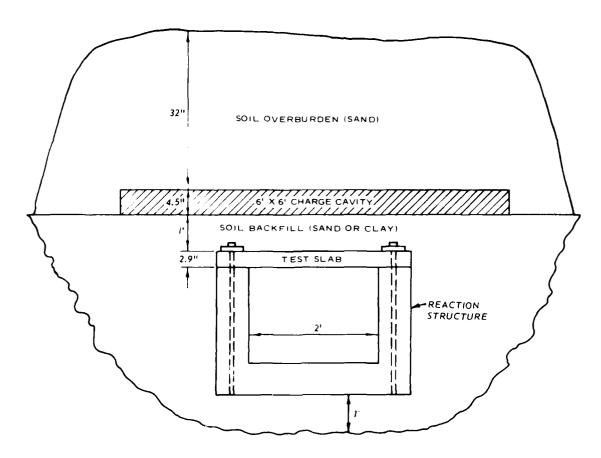


Figure 3.6. Foam HEST configuration.

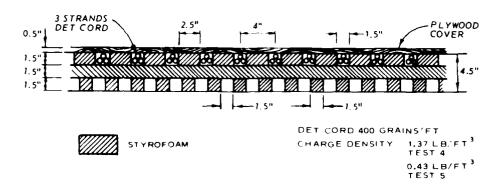


Figure 3.7. Foam HEST charge cavity, Tests 4 and 5.

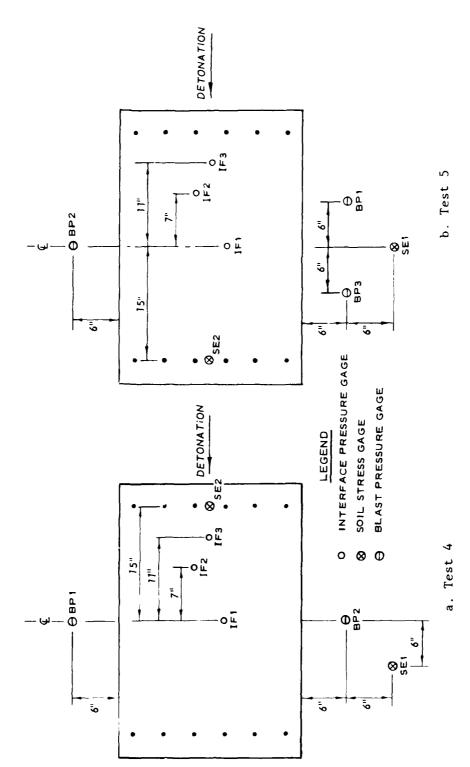


Figure 3.8. Instrumentation for Tests 4 and 5.

CHAPTER 4

TEST RESULTS

4.1 DATA

Three static tests and two dynamic, Foam HEST, tests were conducted. The static tests conducted were surface flush, and buried 1 foot deep in either a high-shear-strength sand backfill, or a low-shear-strength clay backfill. The two dynamic tests repeated the sand and clay backfill conditions. Tests similar to these were conducted in the SBS Research Program at WES and are reported in References 1-7.

All data were recorded on magnetic tape and later reduced to a digital format. A "sample and hold" technique was used to digitize the static test data. The water pressure, as recorded from gage P1, was chosen as the reference channel and all static test data are displayed with P1 as the ordinate. The dynamic test data were digitized at a rate of 100,000 Hz.

4.2 STATIC TEST DATA

4.2.1 Surface-Flush Static Test (Test 1)

This test was conducted with no soil cover on the slab in order to experimentally determine its ultimate capacity without the complicating effects of soil-structure interaction.

The test was interrupted at approximately 163 psi and the slab was unloaded. The applied pressure (water pressure) as a function of centerline deflection is shown in Figure 4.1. The poor data record in Figure 4.1 resulted because the measured deflections were very small relative to the calibration value of 3.80 inches. The measured deflection of the center of the slab at 163 psi was approximately 0.11 inch. Inspection of the slab following this initial loading revealed tension cracks near each supporting edge and the beginning of a compression failure along the top center of the slab. A photograph of the slab in the test chamber following the initial loading is shown in Figure 4.2.

This same test slab was then loaded to its maximum capacity of 174 psi as shown in Figure 4.3. The deflection at ultimate capacity is found from Figures 4.1 and 4.3 to be approximately 0.21 inch; i.e., 0.11 inch from

Figure 4.1 plus 0.10 inch from Figure 4.3. The second loading was discontinued at approximately 110 psi and the slab was unloaded.

In a third loading, shown in Figure 4.4, the slab was loaded to collapse. Note that the permanent deflection from the first two loadings, approximately 0.25 inch, should be added to the deflections measured in the third loading (Figure 4.4) to determine the total displacements.

The slab failed in a classic three-hinge mechanism as shown in Figure 4.5. Centerline deflection was approximately 4.5 inches where it came to rest on supports inside the reaction structure (see Figure 4.14 for similar failure in Test 2). The bottom reinforcing steel was broken along the entire width of the center of the slab.

4.2.2 Static Test in Sand (Test 2)

Test 2 was a static test of the slab buried 1 foot deep in the noncohesive sand backfill described in Section 2.3. The centerline deflection of
the slab as a function of the water pressure over the soil surface is shown
in Figure 4.6. The ultimate capacity of the soil-structure system was
approximately 835 psi, an almost fivefold increase over the ultimate capacity of the surface-flush slab. This dramatic increase in capacity is due to
the soil-structure interaction phenomenon known as soil arching. Soil arching, again, is the ability of a soil to transfer loads by means of a system
of shear stresses from one location to another in response to a relative displacement between the locations. Data reported in Reference 1 from a similar
test on a reinforced concrete box structure also showed an approximately
fivefold increase in capacity due to soil arching.

Data from the interface pressure gages IF1, IF2, and IF3 are shown in Figures 4.7, 4.8, and 4.9. IF1 (Figure 4.7) was located at the center of the slab, IF2 (Figure 4.8) at the quarter point of the slab, and IF3 (Figure 4.9) approximately 11 inches from the center of the slab as shown in Figure 3.4. Comparing these interface pressure data records clearly shows the effect of soil arching on the pressure transmitted to the slab. The maximum pressure occurring at the center of the slab (Figure 4.7) was approximately 93 psi and decreased to almost zero before the slab collapsed at an applied surface pressure (water pressure) of 835 psi. The maximum pressure occurring at the quarter point (Figure 4.8) was approximately 550 psi, and near the edge of the slab (Figure 4.9) the maximum pressure was 972 psi. Thus, the effect of

soil arching was to transfer the load away from the relatively flexible center of the slab toward the relatively stiff supports.

Soil stress gages were placed just over the slab in positions similar to the interface gages (Figure 3.4). Data records from these gages (SE1, SE2, and SE3) are shown in Figures 4.10, 4.11, and 4.12, respectively. These data show load distribution on the roof similar to that shown by the interface pressure data. The relatively low stress recorded on SE3 (Figure 4.12) is unexplained; however, stress recorded by SE1 (Figure 4.10) over the center, SE2 (Figure 4.11) over the quarter point, and SE4 (Figure 4.13) over the support indicates that soil arching did occur. Data from SE4 (Figure 4.13) indicate a maximum pressure over the support of approximately 1,600 psi, almost twice the applied surface pressure. Load was being transferred, through soil arching, from the area over the slab and from the free field near the relatively stiff reaction structure.

A posttest photograph of the slab is shown in Figure 4.14. The three-hinge failure mechanism was very similar to the failure mechanism in Test 1. Again, the slab came to rest on supports inside the reaction structure at a deflection of about 4.5 inches.

Note the compression failure along the bottom of the slab near each support in Figure 4.14. This was typical of all of the tests and occurred because the rigidly clamped supports created large compressive membrane stresses as the slab began to deflect. These compressive membrane stresses acted to significantly increase the ultimate capacity of the slab and to cause the relatively rapid decrease in strength after the maximum capacity had been attained.

4.2.3 Static Test in Clay (Test 3)

Test 3 was a static test of the slab buried under 1 foot of the cohesive, low-shear-strength clay backfill described in Section 2.4. A clay backfill was chosen for this test to investigate soil-structure interaction in two extremes of soil materials, i.e., high-shear-strength sand in Test 2 and a low-shear-strength clay in Test 3. As shown in Figure 4.15, the ultimate capacity of the soil-structure system was approximately 174 psi, the same as it was in the surface-flush case, Test 1. This indicates that much less soil arching occurred in the clay than in the sand, and the interface pressure data records in Figures 4.16, 4.17, and 4.18 confirm this. In Reference 5, a

similar test on a box-type structure in a clay backfill indicated that very little soil arching had occurred. Maximum pressures on the slab occurred at maximum surface pressure (water pressure) and were approximately 156 psi at the center, 174 psi at the quarter point, and 181 psi near the support, as shown in Figures 4.16, 4.17, and 4.18, respectively. The soil stress directly over the slab support is shown in Figure 4.19. These data clearly indicate that some soil arching did occur.

The slab failed in a three-hinge mechanism as did the slabs in Tests 1 and 2. A posttest photograph of the slab is shown in Figure 4.20. The slab again came to rest on supports inside the reaction structure at a centerline deflection of approximately 4.5 inches.

4.3 DYNAMIC TEST DATA

Two dynamic tests were conducted at the Big Black Test Site near Vicksburg, Miss. Both tests employed the reaction structure used in the static tests (Figure 3.2). The simulated nuclear airblast overpressures in these tests were generated with the Foam HEST described in Section 3.5 (Figure 3.7). Similar dynamic tests on box-type structures are described in References 2 and 5.

4.3.1 Dynamic Test in Sand (Test 4)

The test element for Test 4 was identical to the slabs tested statically and was buried under 1 foot of sand as shown schematically in Figure 3.6. Peak airblast pressure was approximately 3,300 psi. A charge density of 1.37 lb/ft³ was used in the Foam HEST. The airblast data measured in the charge cavity by blast pressure gage No. 1 (BP1) are shown in Figure 4.21. Data from BP2 were not recovered.

The nuclear weapon yield and overpressure simulation were determined by comparing nuclear overpressure-time histories as defined in Reference 17 with 2 and 10 ms (taking time equal to zero at peak pressure) of the airblast pressure-time history recorded during the experiment. Best-fit nuclear overpressure-time histories for the airblast records were determined in a least-squares sense using the computer code described in Reference 18. The approximate nuclear weapon yield and overpressure simulated in Test 4 were 0.027-KT and 3,300 psi, respectively. The airblast and impulse data records with the best-fit nuclear pressure-time and impulse-time histories

superimposed on the data are shown in Figure 4.22.

Posttest photographs of the slab are shown in Figures 4.23 and 4.24. Note that in the dynamic failure mechanism three hinges formed as they did in the three static tests. The damage level in this test was higher than in the static tests, i.e., more concrete was broken up and crushed, indicating that the dynamic pressure level may have been higher than the minimum collapse pressure. However, since catastrophic collapse of the slab at both supports did not occur, it was not a significant overtest. The center of the slab came to rest on struts inside the reaction structure at a deflection of approximately 4 inches.

Interface pressure records are shown in Figures 4.25, 4.26, and 4.27. Note that IF1 (Figure 4.25) was broken very early in the test; however, since a partial data record was recovered, the data are included. The data records for the three gages are very similar, showing approximately 2,000-psi peak pressure across the "roof" of the structure, if the initial spike is disregarded. The pressure across the roof fell to zero in approximately 1 ms. Since the natural period of the structure is approximately 4.3 ms, it is unlikely that a flexural failure occurred during the first millisecond. The closeup photograph in Figure 4.24 indicates that a partial shear failure may have occurred. An early-time shear failure (occurring during the first millisecond of loading) could have caused the load to be arched from the deflecting roof onto the slab supports. The data from the soil stress gage (SE2) positioned over one support as shown in Figure 4.29 does not show as sudden or as great a drop in pressure as was seen across the roof on the IF gages. It measured significantly more impulse over the roof support than the IF gages measured over the roof. Also, the impulse recorded by the free-field soil stress gage (SE1, Figure 4.28) was much less than the impulse recorded over the slab support on SE2. This indicates that soil arching did occur, probably from both the free field around the structure and from the deflecting slab area onto the relatively stiff slab supports. Data indicating the phenomenon of dynamic soil arching are well documented in References 2, 4, 5, and 6.

The centerline deflection of the slab shown in Figure 4.30 does not show a sudden early-time shear failure. However, the maximum frequency this gage can respond to is approximately 100 Hz. The gage is a relatively long slender probe primarily designed for static testing and cannot respond to deflection

occurring in the millisecond range; thus, it would not have registered an early-time partial shear failure. The maximum deflection of approximately 3 inches indicated in Figure 4.30 is most likely where the gage probe bent and the gage failed.

4.3.2 Dynamic Test in Clay (Test 5)

The test element design, reaction structure, test configuration, and instrumentation for Test 5 (dynamic test in clay) are shown in Figures 2.1, 3.2, 3.7, and 3.8, respectively. The slab was buried under 1 foot of the same low-shear-strength clay backfill used in Test 3. Material properties for the clay backfill are given in Section 2.4. Because very little dynamic soil arching was expected in the low-shear-strength backfill, the HEST test for Test 5 was designed to produce a lower pressure than that for Test 4. The peak airblast pressure recorded in Test 5 was approximately 860 psi. A charge density of 0.43 lb/ft³ was used in the Foam HEST. Electronic noise occurred on most data records in Test 5; therefore, in most cases, both unfiltered and filtered versions of the data are given. Airblast data measured in the charge cavity are shown in Figures 4.31, 4.32, and 4.33. Data from BP2 were not recovered and BP3 (Figure 4.32) appears to have recorded more reliable data throughout the test than BP1. The nuclear weapon yield and overpressure that best fit (in a least-squares sense) the first 10 ms of data from gage BP3 were determined using the procedure described in Reference 18. As shown in Figure 4.33, the weapon yield simulated in Test 5 was approximately 0.010 KT at a peak overpressure of about 860 psi. Impulse-time histories comparing the integration of the measured data with the simulated weapon are shown in Figure 4.34. Clearly, the yield and overpressure combination shown in Figure 4.33 is a good fit to the data. However, it should be noted that many other yield-overpressure combinations were also well simulated in this experiment. For example, a best fit in the sense of Reference 18 is shown for 2 ms of data from BP3 in Figure 4.35; i.e., a yield of 0.047 KT at a peak overpressure of 447 psi. In general, the best fit will vary with the length of data record chosen. Also, very good (but not best) fits exist at larger yields with lower pressures and at smaller yields with higher pressures than the best-fit weapon. See References 14, 15, and 16 for more information on using the Foam HEST for nuclear overpressure simulations.

Posttest photographs of the Test 5 slab are shown in Figure 4.36. The

classic three-hinge failure mechanism is again evident. Maximum deflection was 0.82 inch and occurred at about 10 ms, as shown in Figure 4.37.

Data from interface pressure gages IF1, IF2, and IF3 are shown in Figures 4.38, 4.39, and 4.40, respectively. These data, along with soil stress data (Figure 4.42) from gage SE2, which was over the slab support, indicate that almost no dynamic soil arching occurred in the low-shear-strength clay backfill. Soil stress gage SE1 measured the free-field soil stress, as shown in Figure 4.41. The data record in Figure 4.42 from SE2 was discontinued at about 6 ms because the gage malfunctioned.

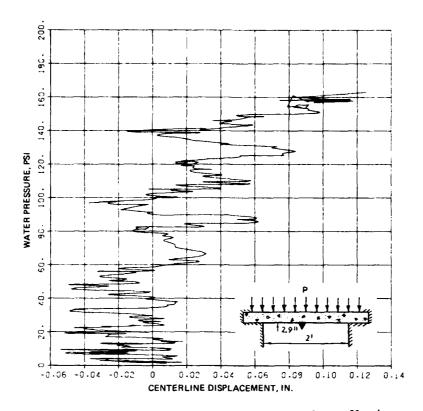


Figure 4.1. Initial loading of surface-flush static test.

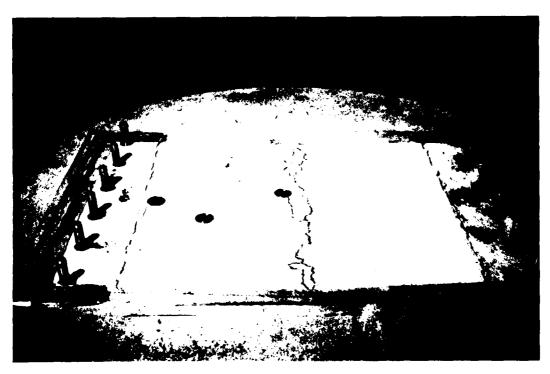


Figure 4.2. Surface-flush static test slab following initial loading.

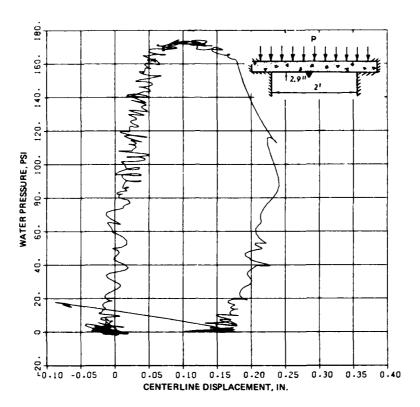


Figure 4.3. Ultimate capacity of surface-flush slab.

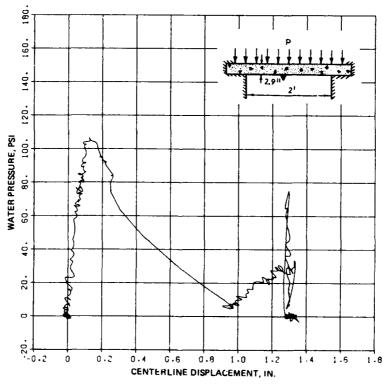


Figure 4.4. Collapse loading of surface-flush slab.

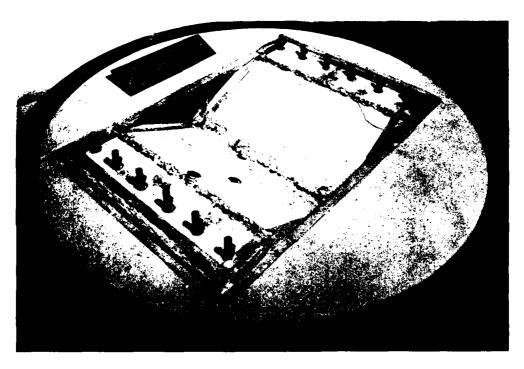


Figure 4.5. Failure of surface-flush static test slab.

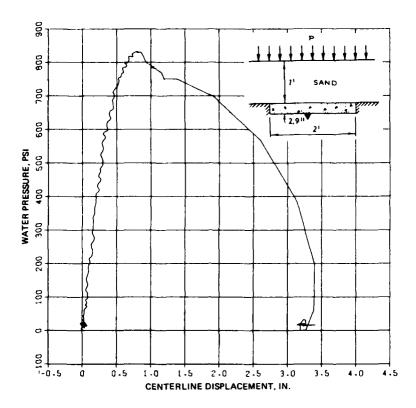


Figure 4.6. Resistance for sand-backfill static test.

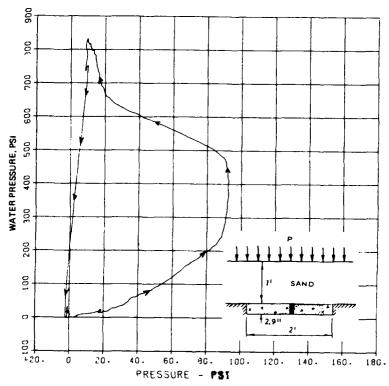


Figure 4.7. Centerline interface pressure in sand-backfill test.

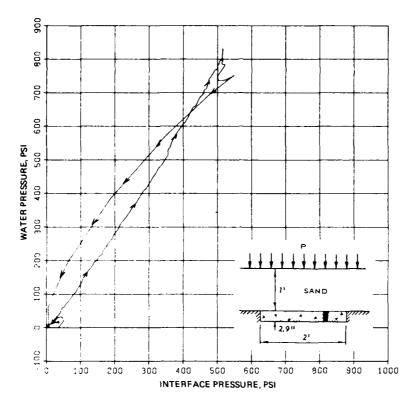


Figure 4.8. Quarter-point interface pressure in sand-backfill test.

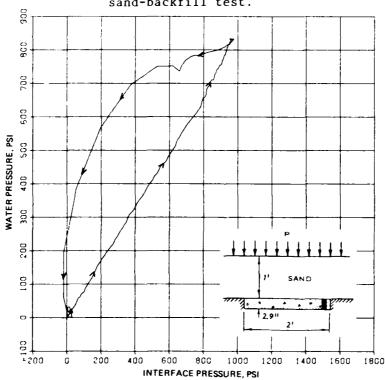


Figure 4.9. Interface pressure at end of clear span in sand-backfill test.

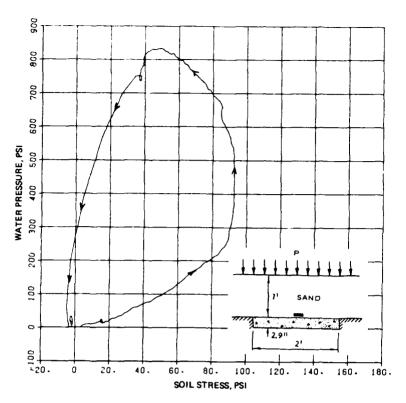


Figure 4.10. Centerline soil stress in sand-backfill test.

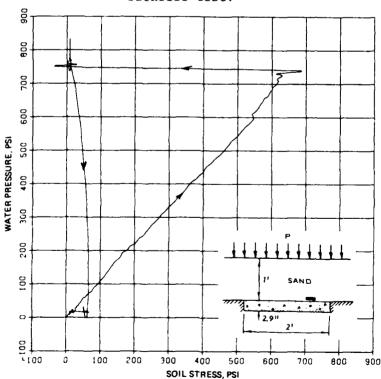


Figure 4.11. Quarter-point soil stress in sand-backfill test.

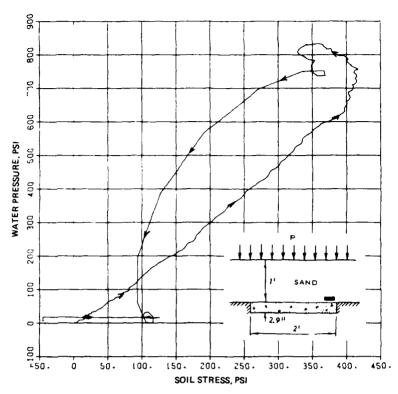


Figure 4.12. Soil stress near end of clear span in sand-backfill test.

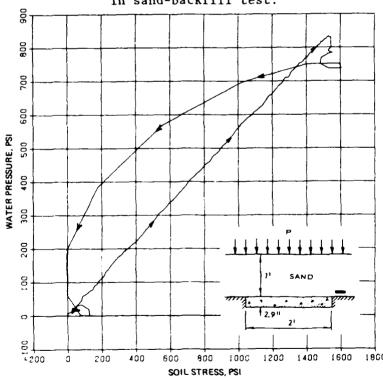


Figure 4.13. Soil stress over support in sand-backfill test.

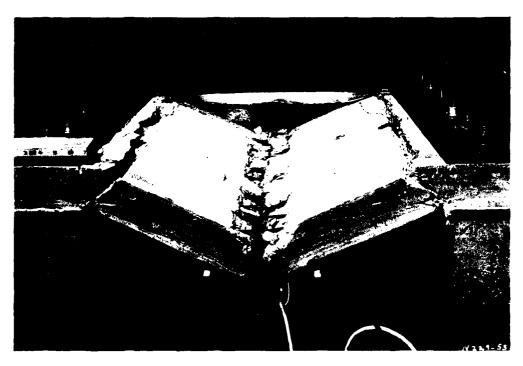


Figure 4.14. Posttest photograph of the sand-backfill static test slab.

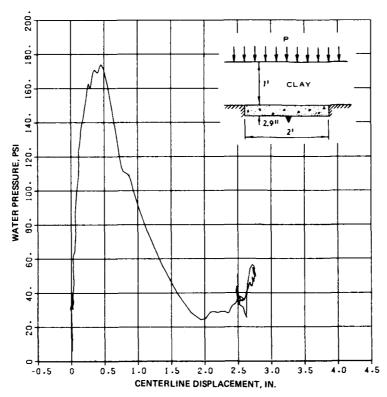


Figure 4.15. Resistance in static clay-backfill test.

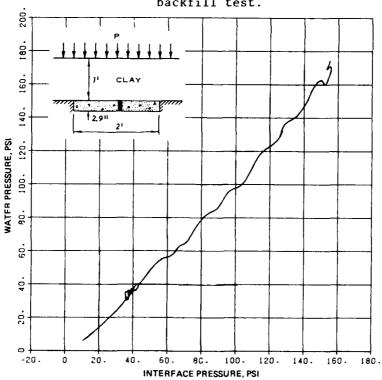


Figure 4.16. Centerline interface pressure in static clay-backfill test.

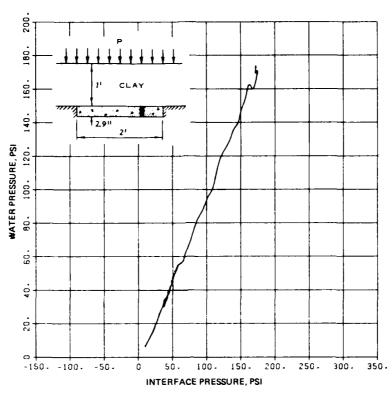


Figure 4.17. Quarter-point interface pressure in static clay-backfill test.

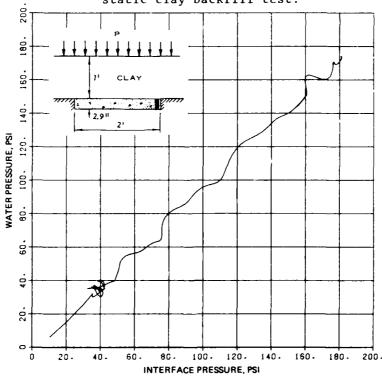


Figure 4.18. Interface pressure near support in static clay-backfill test.

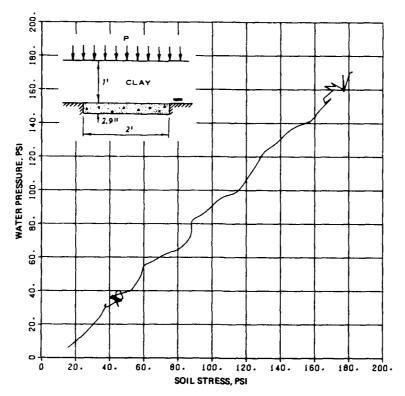


Figure 4.19. Soil stress over slab support in static clay-backfill test.



Figure 4.20. Posttest photograph of slab in static clay-backfill test.

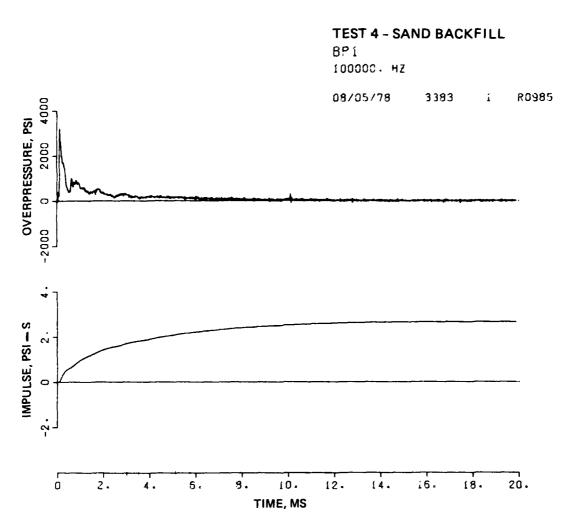
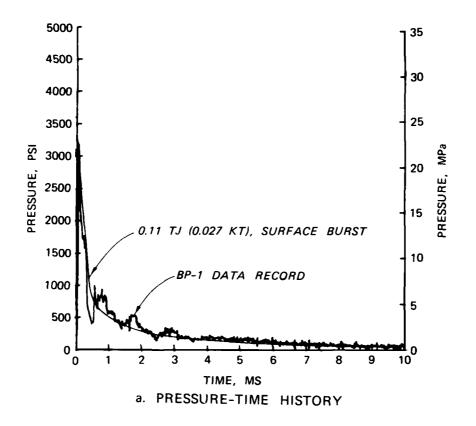


Figure 4.21. Dynamic overpressure record in Test 4.



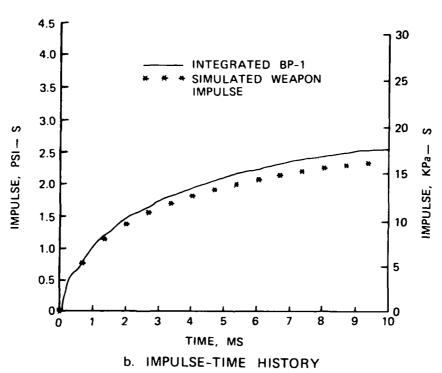


Figure 4.22. Airblast pressure from Test 4 and weapon simulation.

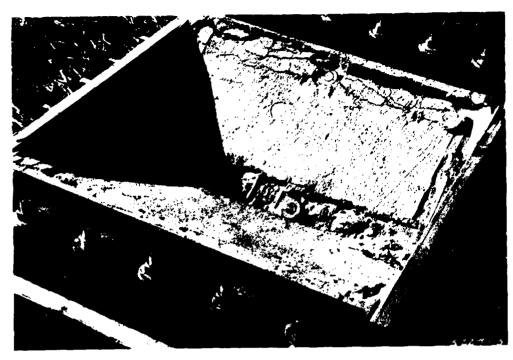


Figure 4.23. Posstest view of Test 4 slab failure.



Figure 4.24. Closeup view of Test 4 slab.

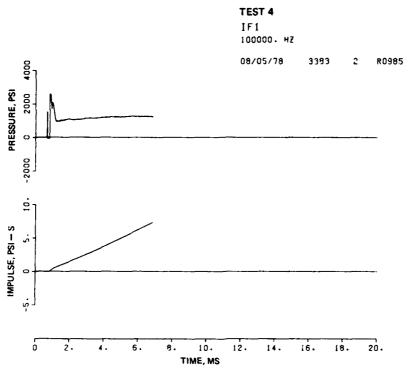


Figure 4.25. Interface pressure at the center of the slab in Test 4.

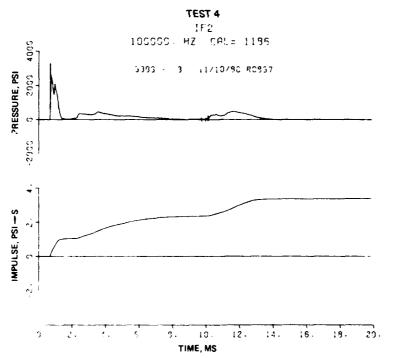


Figure 4.26. Interface pressure 7 inches from the center of the slab in Test 4.

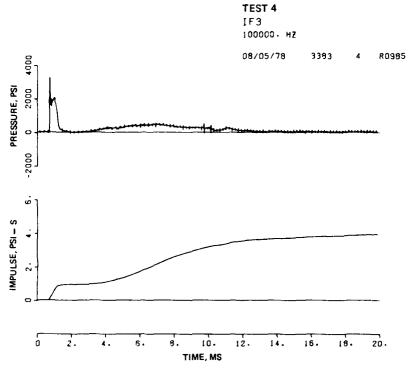


Figure 4.27. Interface pressure 11 inches from the center of the slab in Test 4.

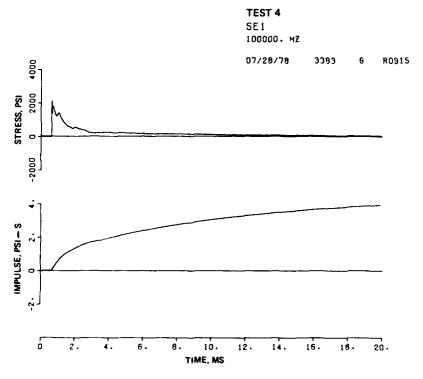


Figure 4.28. Free-field soil stress in Test 4.

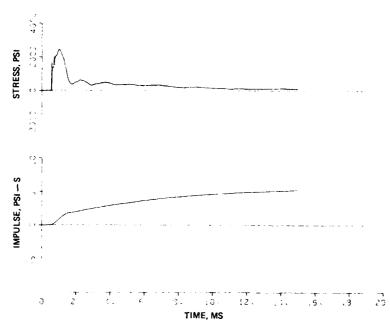


Figure 4.29. Soil stress over the slab support in Test 4.

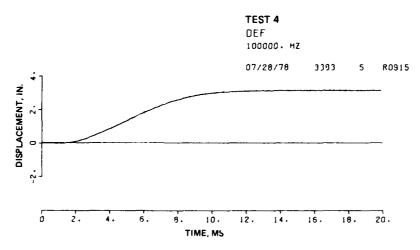
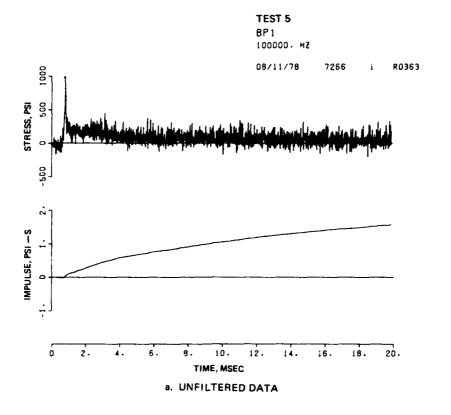


Figure 4.30. Centerline deflection of slab in Test 4.



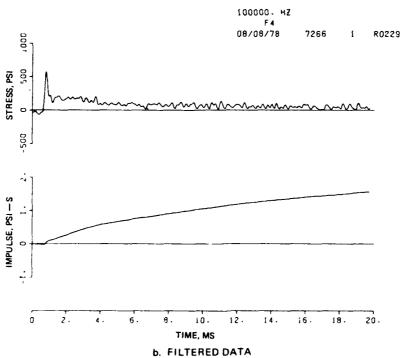
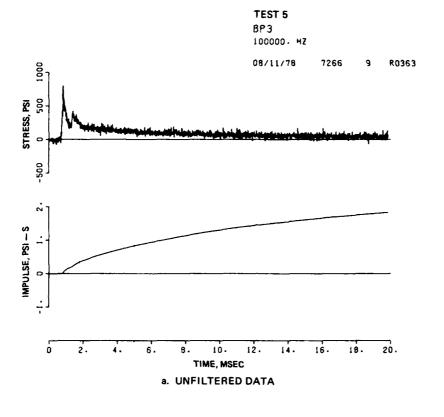


Figure 4.31. Airblast pressure from Test 5 measured by BP1.



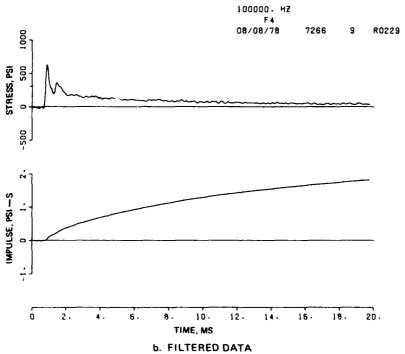


Figure 4.32. Airblast pressure from Test 5 measured by BP3.

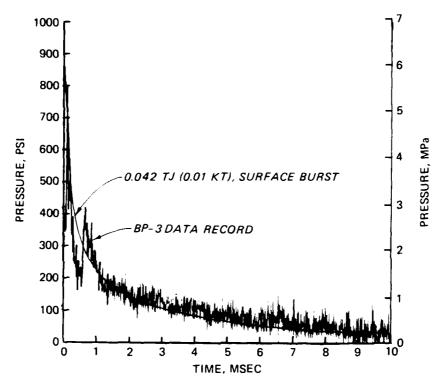


Figure 4.33. Pressure-time records and simulation, Test 5.

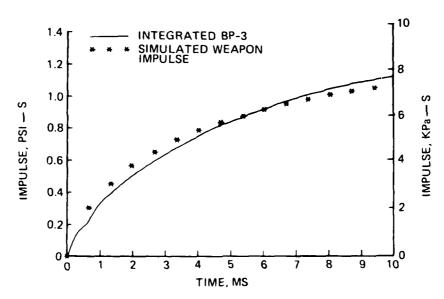
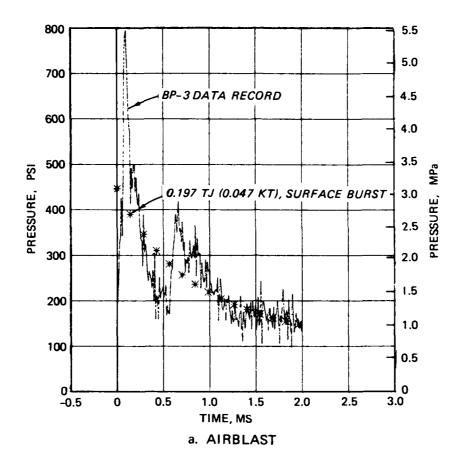


Figure 4.34. Impulse-time records and simulation, Test 5.



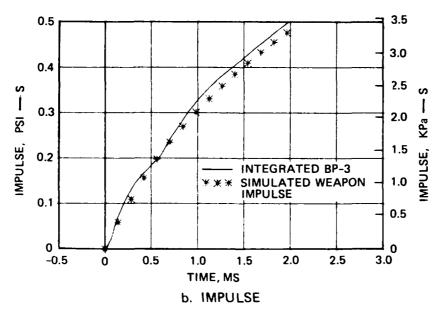
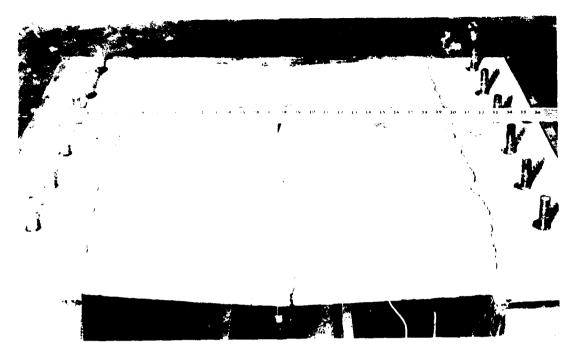
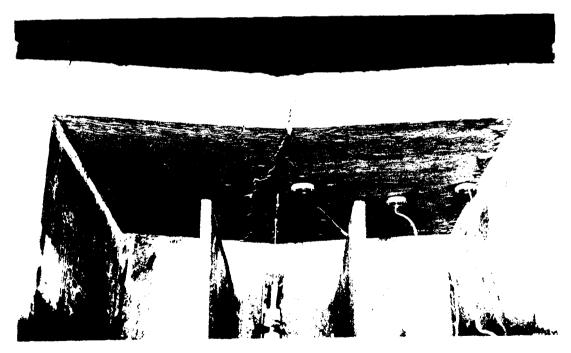


Figure 4.35. Alternate Test 5 simulation.



a. Surface of slab



b. Underside of slab

Figure 4.36. Posttest photographs of Test 5 slab.

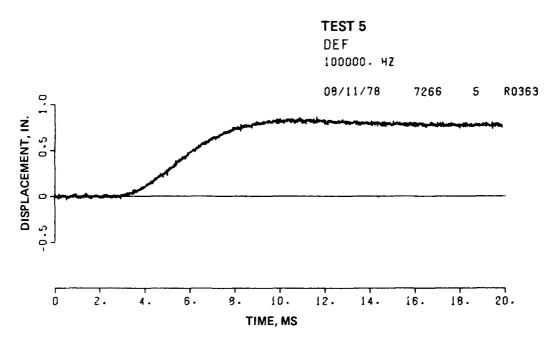
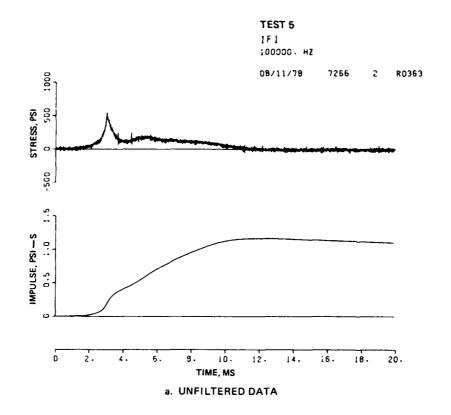


Figure 4.37. Test 5 deflection record.



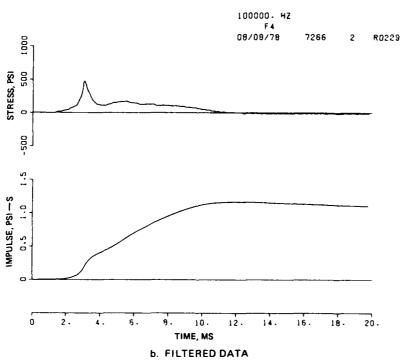
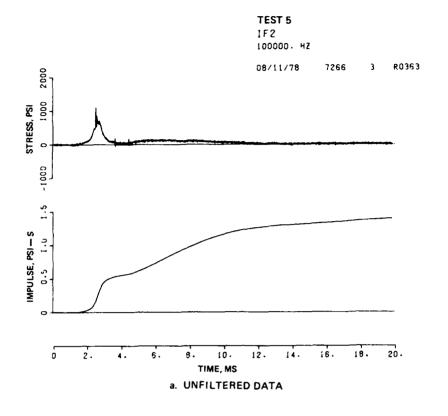


Figure 4.38. IF1 interface data from Test 5.



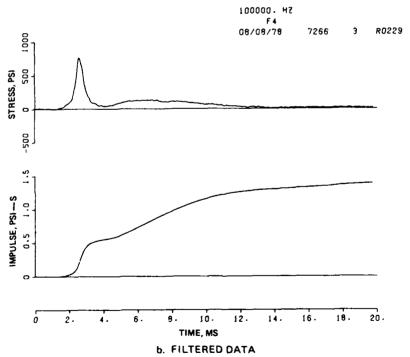
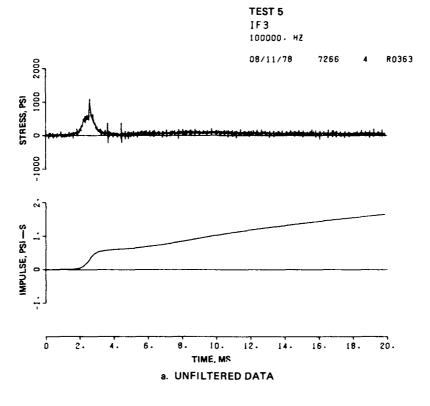


Figure 4.39. IF2 interface data from Test 5.



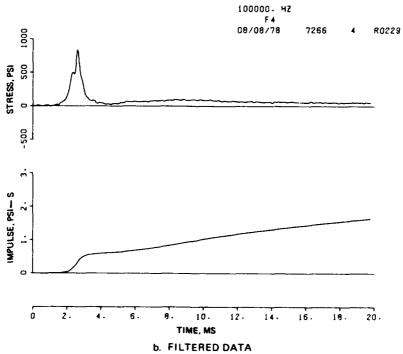
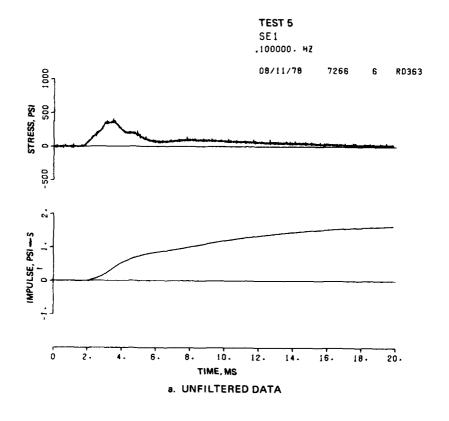


Figure 4.40. IF3 interface data from Test 5.



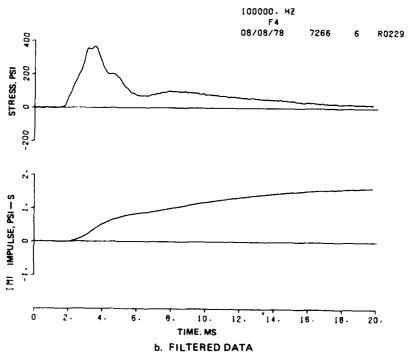


Figure 4.41. SE1 soil stress data from Test 5.

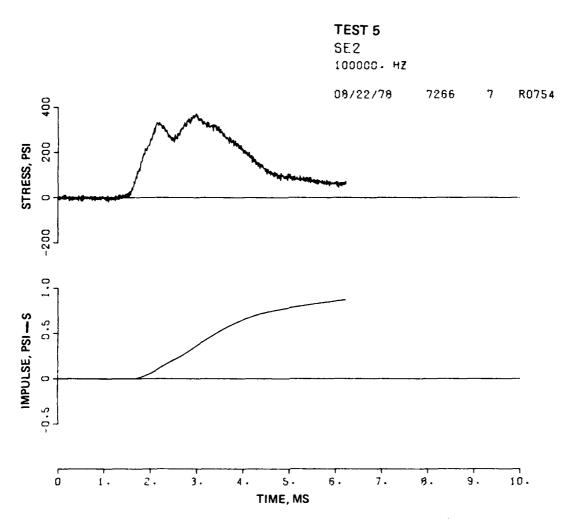


Figure 4.42. SE2 soil stress data from Test 5 (record discontinued because of gage malfunction).

CHAPTER 5

ANALYSIS

Two important parameters affecting the maximum capacity of the elements used in these tests were soil arching and compressive membrane stresses imposed by the rigid support conditions of the reaction structure. Support conditions, and thus compressive membrane stresses, were the same for each test; and the rigidity of the reaction structure prevented active lateral earth pressure, another possible variable, from contributing to the in-plane thrust in the test slabs. Therefore, the only parameter variation between tests was soil arching. Similar tests on box elements are reported in References 1-7.

5.1 MAXIMUM RESISTANCE

The maximum resistance to a uniformly applied load for a one-way fixed slab, from Reference 19, is

$$P_f = 7.2(\rho_c + \rho_e)f_v(d/L)^2$$
 (5.1)

where

 P_f = uniform load resistance based on flexural capacity

 ρ_c = tensile reinforcing steel ratio at midspan

 $\rho_{\rm p}$ = tensile reinforcing steel ratio at end

 f_{u} = reinforcement steel yield stress

d = depth to center of reinforcing steel

L = clear span of the slab

From Equation 5.1, the ultimate capacity of the slab element is 65 psi. However, Equation 5.1 does not account for the compressive membrane action produced by the rigid support conditions in these tests. This compressive membrane stress can dramatically increase ultimate capacity by forcing the concrete near the supports to crush. This effect can be important in slabs with relatively low reinforcement ratios but is negligible for heavily reinforced slabs. The effect of this compressive membrane stress on ultimate capacity is investigated in some detail by Keenan (Reference 20) and by Parks (References 21-23).

The ultimate capacity, $\,\mathbf{q}_{u}$, of the test slabs, including compressive membrane effects, from Reference 20 is

$$q_{u} = \frac{8}{\left(\frac{L}{t}\right)^{2}} \left[2 \left(\frac{M_{u}}{t^{2}}\right) - \frac{Z_{u}}{t} \left(\frac{N_{u}}{t}\right) \right] = 180 \text{ psi}$$
 (5.2)

where

$$\frac{Z_{u}}{t} = 1 - \sqrt{1 - 1/2 \left(\frac{L}{t}\right)^{2} \left[s(1 + \varepsilon_{u}) + \varepsilon_{u}\right]}$$

 Z_{ij} = midspan deflection at crushing strain of the concrete (0.206 inch)

t = thickness of slab

L = clear span of :lab

s = ratio of total horizontal edge movement to clear span

 ε_{n} = crushing strain of concrete

$$\frac{N_u}{t} = f_c'' \left[K_1 \left(\frac{c}{t} \right) - \left(\frac{pf_s - p'f_s'}{f_c''} \right) \frac{d}{t} \right]$$

 N_u = self-generated thrust at middepth in the slab when the concrete crushes (5,992 lb/in.)

 $f_c'' = 0.85 f_c' = compressive strength of concrete in flexure$

 K_1 = ratio of average stress to peak stress, f_c'' , in concrete

c = depth to neutral axis when concrete crushes (1.40 inches)

 $p = ratio of tension reinforcement = A_s/d$

 $f_{c} = stress$ in tension reinforcement when concrete crushes

=
$$E_s \epsilon_u \left(\frac{d}{c} - 1\right) \le f_y = 85,934 \text{ psi } (f_y = 90,000 \text{ psi})$$

 $p' = ratio of compression reinforcement = A'_s/d$

 f'_{s} = stress in the compression reinforcement when concrete crushes

$$= E_u \epsilon_u \left(1 - \frac{d'}{c}\right) \leq f_y = 77,097 \text{ psi}$$

A_c = area of tension reinforcement

d = distance from compression edge of slab to centroid of tension
reinforcement

 A_c' = area of compression reinforcement

$$\frac{c}{t} = 1/2 - 1/4 \left(\frac{Z_u}{t}\right) - \frac{s\left(\frac{L}{t}\right)^2}{8\left(\frac{Z_u}{t}\right)}$$

 E_{c} = modulus of elasticity of reinforcing steel

d' = distance from compression edge of slab to centroid of compression reinforcement

$$\frac{M_u}{t^2} = pf_s\left(\frac{d}{t}\right)\left(\frac{d}{t} - \frac{1}{2}\right) + f_c'' K_1\left(\frac{c}{t}\right)\left(\frac{1}{2} - K_2\frac{c}{t}\right) + p'f_s'\left(\frac{d}{t}\right)\left(\frac{1}{2} - \frac{d'}{t}\right)$$

 $M_u = \text{moment resistance of hinge sections under a thrust } N_u = (7119 in-lb/in)$

 K_2 = coefficient-defining fraction of the depth measured from the extreme fiber to the resultant force in the concrete

The ultimate capacity of 180 psi predicted for the slab by Equation 5.2 agrees very well with the capacities as determined experimentally in Tests 1 and 3 (static surface flush and clay backfill tests). Under conditions where little or no soil arching could occur, the compressive membrane forces acted to almost triple the capacity of the slab in its unrestrained condition represented by Equation 5.1.

5.2 SOIL ARCHING

Soil arching may act in a large sense and cause a stress change throughout a volume of soil because the structure located therein exhibits a different compressibility than does the surrounding soil; or it may act in a local sense, as around a tunnel, and cause a redistribution of stress as various elements of the tunnel attempt to move into or away from the surrounding soil. Embedded structures that are much stiffer than their surrounding medium will tend to attract load. On the other hand, stress will be diverted away from or around embedded structures that are less stiff than their surrounding medium. It is generally called "passive arching" when the load on the structure is greater than the free-field stress and "active arching" when the load on the structure is less than the free-field stress. Experimental data on soil arching can be found in References 1-12.

In Reference 10, McNulty derives an expression for the arching ratio (i.e., the ratio of average pressure on the buried structure to the applied surface pressure) by assuming that a vertical column of soil directly above the structure deforms with the test element. In Figure 5.1, this approach is adapted to a rectangular element to obtain

$$\frac{P_{B}}{P_{S}} = \exp\left[\frac{-2K(\tan\phi)(W+L)H}{WL}\right]$$
 (5.3)

where

 P_{R} = average pressure acting on the roof

 P_{c} = surcharge pressure acting on the soil surface

K = coefficient of lateral earth pressure (ratio of horizontal to vertical pressure in the soil)

 ϕ = the angle of internal friction in the soil

W = width of the roof

L = length of the roof

H = depth of burial

Equation 5.3 does not include cohesive forces in the soil or the weight of the soil. As suggested in References 11 and 24, ϕ should be increased as the ratio of depth-of-burial to span increases, to account for the additional lateral restraint provided by the soil at increasing depth. The variation of ϕ with depth can be represented by the ratio of ϕ_f/ϕ , where ϕ_f is the angle of friction at depth. This ratio varies from 1.0 for structures placed at the ground surface where there is small lateral constraint to 1.5 for a depth of burial (DOB) equal to the width of the structure. At greater depths, the value of ϕ_f/ϕ is assumed to remain approximately 1.5.

For a DOB equal to 0.5L (assuming a linear variation),

$$\frac{\Phi_{\mathbf{f}}}{\Phi} = 1.25$$

Therefore, for Test 2 in a sand backfill,

$$\phi_f = 1.25 \ (35.5 \text{ degrees})$$

= 44.38 degrees

Using

K = 0.5 (from Reference 9) and $\,\varphi$ = 44.4 degrees Equation 5.3 gives

$$\frac{P_B}{P_S} = 0.38$$

Therefore, at a maximum surface pressure of 840 psi, the average pressure predicted by Equation 5.3 on the element is 320 psi. As discussed in References 1

and 7, soil arching produces a nonuniform distribution of pressure on the structure, very low in the center and high near the supports. As shown in Figure 4.7, the interface pressure in Test 2 at the center of the roof when the structure failed was less than 20 psi. This can explain the difference between the ultimate capacity observed in Test 1 (surface flush) of about 174 psi and the average pressure in Test 2 of about 320 psi. In fact, in a fully plastic response mode, a one-way slab, responding in flexure, will resist twice as much total load if it is distributed parabolically as it will resist if the load is uniformly distributed (Reference 7).

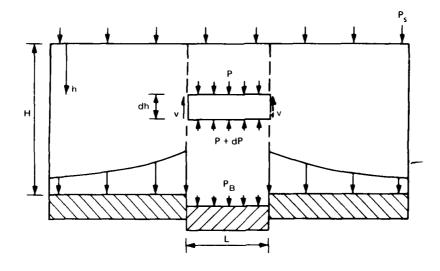
5.3 WEAPON SIMULATION

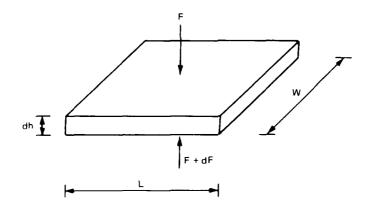
The objective of this study was to investigate the effect of earth cover on structural response to nuclear-type overpressures. Therefore, it is important that the Foam HEST produce a structural response similar to that produced by the simulated nuclear overpressure. In Figures 5.2, 5.3, and 5.4, dynamic load factors computed from blast pressures measured in the tests are compared to dynamic load factors computed from pressure time histories for the weapons simulated. In general, the load factors agree within 10 percent at frequencies below 500 Hz. If the structure being tested has important response frequencies above 500 Hz, the high-frequency pressure oscillations in the HEST cavity may cause a problem with nuclear blast simulation. However, as shown by the soil stress data records, most of the high-frequency oscillations in the Foam HEST are damped out in the soil overburden.

5.4 DYNAMIC RESPONSE

A single-degree-of-freedom analytical model was used to compute structural response from the simulated weapon overpressures. Analytical procedures described in Reference 24 were used to attenuate the overpressure through the overburden and compute structural loading. The bilinear resistance function had an elastic deflection of 0.15 inch and a maximum resistance of 180 psi (Equation 5.2). Maximum computed deflection from a 0.027-KT yield at a 3,300-psi peak overpressure (Test 4 simulation), was 128 inches, and from a 0.010-KT yield at an 860-psi peak overpressure (Test 5 simulation) the computed deflection was 13.2 inches. Either of these computed deflections implies total collapse of the slab. The deflection resulting from Test 5 was 0.8 inch rather than the predicted 13.2 inches and the significant overkill

(128-inch deflection) predicted for Test 4 did not occur. Therefore, the analytical procedures described in Reference 25 significantly overpredict structural response under the conditions present here. Analyses of the test data for these and similar experiments using a nonlinear finite element code are given in References 26-28.





$$\begin{split} F &= PWL & dF &= dPWL \\ v &= KP \, Tan \, \, \, \phi & V &= v(2)(w+L)dh \\ \Sigma F_{vert} &= 0 & dP &= \frac{-KP2(tan \, \phi)(W+L)dh}{WL} \, , \, at \, h = 0, \, P = P_s \\ F &= (F+dF) + V \\ dF &= -V & \frac{P_B}{P_s} &= exp \Bigg[\frac{-2K(tan \, \phi)(W+L)H}{WL} \Bigg] \end{split}$$

Figure 5.1. Soil-arching ratio.

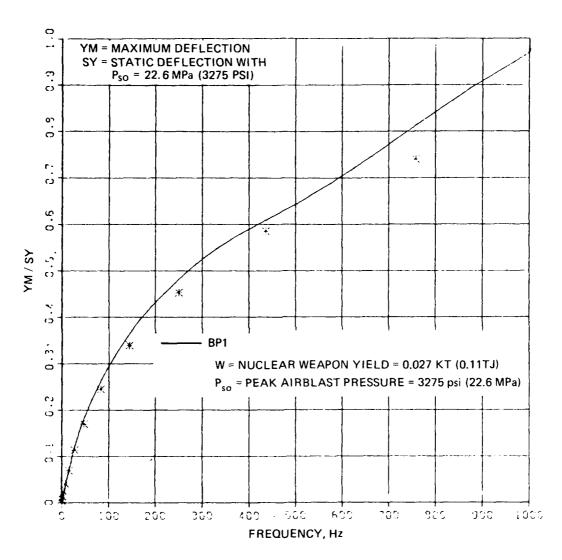


Figure 5.2. Dynamic load factors, BP1, Test 4, 10-ms record.

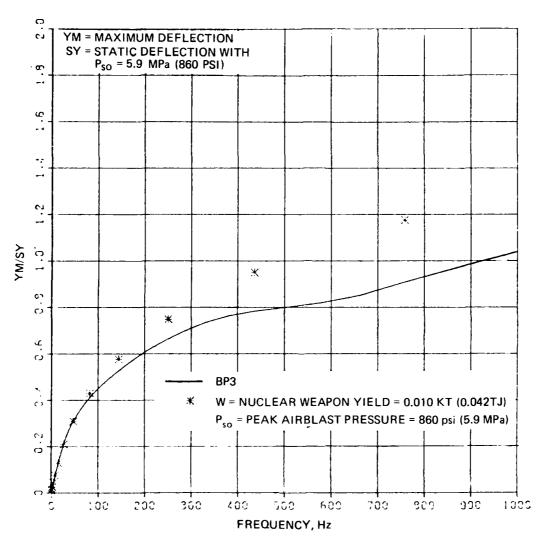


Figure 5.3. Dynamic load factors, BP3, Test 5, 10-ms record.

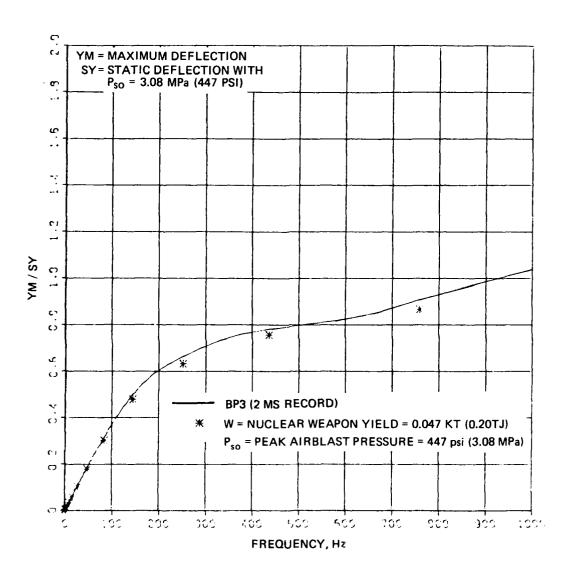


Figure 5.4. Dynamic load factors, BP3, Test 5, 2-ms record.

CHAPTER 6

CONCLUSIONS

The redistribution of pressure on the test slab, i.e., soil arching, caused an approximately fivefold increase in the surface pressure at failure in the static sand-backfill test compared to the static surface-flush and clay backfill tests.

The ratio of the peak surface pressure to the average pressure on the slab, i.e., the arching ratio, was about 0.38 in the static sand-backfill test.

Because of the nonuniform pressure distribution, the average pressure on the slab in the static sand-backfill test at failure was approximately 80 percent greater than the ultimate capacity measured in the surface flush and clay backfill static tests.

Almost no soil arching occurred in the low-shear-strength clay backfill in the static and dynamic tests.

Dynamic soil arching in the sand backfill increased the impulse and the late-time pressure (after about 1 ms) over the slab supports and decreased the late-time pressure on the slab.

Compressive membrane stresses generated by the rigid support conditions produced an approximately threefold increase in the ultimate capacity of the slab over the capacity of a similar less-rigidly restrained slab.

Dynamic load factors computed from the measured airblast data in the Foam HEST and the simulated weapon pressure-time histories compare very well up to about 500 Hz.

Vulnerability analysis methods that do not include dynamic soil-structure interaction effects (i.e., dynamic soil arching) significantly overpredict structural response for flat-roofed shallow-buried structures and underpredict their hardness.

REFERENCES

- 1. S. A. Kiger; "Static Test of a Hardened Shallow-Buried Structure"; Technical Report N-78-7, October 1978; US Army Engineer Waterways Experiment Station, Vicksburg, Miss.
- 2. S. A. Kiger and J. W. Getchell; "Vulnerability of Shallow-Buried Flat-Roof Structures; Foam HEST 1 and 2"; Technical Report SL-80-7, Report 1, September 1980; US Army Engineer Waterways Experiment Station, Vicksburg, Miss.
- 3. J. V. Getchell and S. A. Kiger; "Vulnerability of Shallow-Buried Flat-Roof Structures; Foam HEST 4"; Technical Report SL-80-7, Report 2, October 1980; US Army Engineer Waterways Experiment Station, Vicksburg, Miss.
- 4. J. V. Getchell and S. A. Kiger; "Vulnerability of Shallow-Buried Flat-Roof Structures; Foam HEST 5"; Technical Report SL-80-7, Report 3, February 1981; US Army Engineer Waterways Experiment Station, Vicksburg, Miss.
- 5. J. V. Getchell and S. A. Kiger; "Vulnerability of Shallow-Buried Flat-Roof Structures; Foam HEST 3 and 6"; Technical Report SL-80-7, Report 4, December 1981; US Army Engineer Waterways Experiment Station, Vicksburg, Miss.
- 6. S. A. Kiger and J. V. Getchell; "Vulnerability of Shallow-Buried Flat-Roof Structures; Foam HEST 7"; Technical Report SL-80-7, Report 5, February 1982; US Army Engineer Waterways Experiment Station, Vicksburg, Miss.
- 7. S. A. Kiger and T. R. Slawson; "Vulnerability of Shallow-Buried Flat-Roof Structures"; Technical Report SL-80-7, Report 6 (in preparation); US Army Engineer Waterways Experiment Station, Vicksburg, Miss.
- 8. W. F. Carroll; "Dynamic Bearing Capacity of Soils; Vertical Displacements of Spread Footings on Clay: Static and Impulsive Loadings"; Technical Report No. 3-599, Report 5, September 1963; US Army Engineer Waterways Experiment Station, Vicksburg, Miss.
- 9. G. E. Jester; "An Experimental Investigation of Soil-Structure Interaction in Cohesive Soil"; Technical Report N-70-7, Vol II, March 1970; US Army Engineer Waterways Experiment Station, Vicksburg, Miss.
- 10. J. W. McNulty; "An Experimental Study of Arching in Sand"; Technical Report No. 1-674, May 1965; US Army Engineer Waterways Experiment Station, Vicksburg, Miss.
- 11. R. J. Mosborg and P. M. Talda; "An Experimental Investigation of the Arching Phenomenon Occurring Over a Buried Rectangular Plate"; Technical Report No. AFWL-TR-65-78, 1966; Air Force Weapons Laboratory, Kirtland Air Force Base, N. Mex.
- 12. P. L. Rohmaller; "Arching Effect for Underground Rectangular Structures Subjected to High Static Pressure"; University Microfilms, Inc., University of Michigan, Ann Arbor, Mich.
- 13. W. L. Huff; "Test Devices, Blast Load Generator Facility"; Miscellaneous Paper N-69-1, April 1969; US Army Engineer Waterways Experiment Station, Vicksburg, Miss.
- 14. E. A. Day; "Experimental Program to Demonstrate Feasibility of Foamhest"; Technical Report No DA-352F, 1975; Systems, Science and Software, LaJolla, Calif.

- 15. H. W. Wampler and others; "A Status and Capability Report on Nuclear Airblast Simulation Using HEST"; Proceedings, Nuclear Blast and Shock Simulation Symposium, 28-30 November 1978, Vol I, DNA 4797P-1; Defense Nuclear Agency, Washington, D. C.
- 16. S. A. Kiger; "Use of a Foam HEST to Simulate Low Yield Nuclear Over-Pressures"; Proceedings, Seventh International Symposium on Military Applications of Blast Simulation, 13-17 July 1981, Medicine Hat, Alberta, Canada.
- 17. H. L. Brode; "Height of Burst Effects at High Overpressures"; RM-6301-DASA, 1970 (Revised 1979); The Rand Corporation, Santa Monica, Calif.
- 18. P. F. Mlakar and R. E. Walker; "Statistical Estimation of Simulated Yield and Overpressure"; The Shock and Vibration Bulletin, No. 50, 1980; Shock and Vibration Information Center, Naval Research Laboratory, Washington, D. C.
- 19. R. E. Crawford, C. J. Higgins, and E. H. Bultmann; "The Air Force Manual for Design and Analysis of Hardened Structures"; Technical Report No. AFWL-TR-74-102, 1974; Air Force Weapons Laboratory, Kirtland Air Force Base, N. Mex.
- 20. W. A. Keenan; "Strength and Behavior of Laced Reinforced Concrete Slabs Under Static and Dynamic Loads"; Technical Report No. R620, 1969; Naval Civil Engineering Laboratory, Port Hueneme, Calif.
- 21. R. Parks; "The Ultimate Strength and Long-Term Behavior of Uniformly Loaded, Two-Way Concrete Slabs with Partial Lateral Restraint at All Edges"; Magazine of Concrete Research, Vol 16, No. 48, 1964.
- 22. R. Parks; "Tensile Membrane Behaviour of Uniformly Loaded Rectangular Reinforced Concrete Slabs with Fully Restrained Edges"; Magazine of Concrete Research, Vol 16, No. 46, 1964.
- 23. R. Parks; "The Lateral Stiffness and Strength Required to Ensure Membrane Action at the Ultimate Load of a Reinforced Concrete Slab-and-Beam Floor"; Magazine of Concrete Research, Vol 17, No. 50, 1965.
- 24. Office, Chief of Engineers, Department of the Army; "Designing Facilities to Resist Nuclear Weapons Effects"; Technical Manual No. TM-5-858-3, 1977; Washington, D. C.
- 25. J. D. Haltiwanger, W. J. Hall, and N. M. Newmark; "Approximate Methods for the Vulnerability Analysis of Structures Subjected to the Effects of Nuclear Blast"; Report No. U-275-76, 1976; N. W. Newmark Consulting Engineering Services, Urbana, Ill.
- 26. R. Murtha; "An Assessment of Structural Collapse Predictions for Reinforced Concrete Beams Using ADINA"; TM No. 51-79-16, 1979; Civil Engineering Laboratory, Port Hueneme, Calif.
- 27. R. Murtha and J. Crawford; "Analysis of Static Test of a Hardened Shallow-Buried Structure"; TM 51-79-05, 1979; Civil Engineering Laboratory, Port Hueneme, Calif.
- 28. R. Murtha and J. Crawford; "Updated Static Analysis of Hardened Shallow-Buried Structures"; TM 80-13, 1980; Civil Engineering Laboratory, Port Hueneme, Calif.

DISTRIBUTION LIST

DEPARTMENT OF DEFENSE

Assistant to the Secretary of Defense, Atomic

ATTN: Donald R. Cotter

Director, Defense Advanced Research Projects

Agency

ATTN: Technical Library

Director, Federal Emergency Management Agency ATTN: OMR/Administrative Office

Defense Technical Information Center, Cameron Station

2 cy ATTN: DDAB/Mr. Harry A. Schrecengost, Jr.

Director, Defense Intelligence Agency

ATTN: DT-2, Weapons & Systems Division DB-4C

Technical Library

Carl Wiehle

Director, Defense Nuclear Agency

ATTN: STSI (Archives)

STTL (Technical Library)

SPSS 2 cv

DDST

SPTD/Tom Kennedy

SPSS/Dr. Kent L. Goering

SPSS/MAJ E. Furbee

TISI

DSNS/MAJ George Flowers Mr. Cliff McFarland

Director of Defense Research and Engineering

ATTN: Dep Dir, Strategic Systems Dep Dir, Tactical Warfare

Interservice Nuclear Weapons School

ATTN: Technical Library

Chairman, Department of Defense Explosives

Safety Board

ATTN: Dr. Tom Zaker

Director, Joint Strategic Target Planning Staff

ATTN: Science and Technology Information

Library

Mr. Bob Rautenberg

Commander, Field Command, Defense Nuclear Agency

ATTN: FCTA-D

Oak Ridge National Laboratory

ATTN: Dr. Conrad Chester

U. S. Department of Energy

ATTN: John Filey/FCMD

L. M. Paradee John J. Schinkle

DEPARTMENT OF THE ARMY

Commander, U. S. Army Ballistic Missile Defense Systems Command

ATTN: BMDSC-TEN/Noah J. Hurst

BMDSC-HS

DEPARTMENT OF THE ARMY (Continued)

Office, Chief of Engineers, Department of

the Army

2 cy ATTN: DAEN-ASI-L DAEN-MPE-D

DAEN-RDL

DAEN-ZCM/Mr. Swain

Office, Chief of Engineers, Engineers Study Group

ATTN: DAEN-FES/Mr. George H. Orrell

Commander, Harry Diamond Laboratories

ATTN: AMXDO-NP

AMXDO-TI, Technical Library DELHD-N-EM/Mr. R. Pfeffer

Office, Chief of Research, Development, and

Acquisition

ATTN: DAMA-CSM

G. A. Hegemier, UCSD/S3

Commanding Officer, Picatinny Arsenal

ATTN: P. Angelloti

Director, U. S. Army Ballistic Research

Laboratories

2 cy

ATTN: VLD/Steve Zardas

J. H. Keefer

DRDAR-BLT/Mr. C. W. Kitchens

AMXBR-X/Mr. J. J. Meszaros

Technical Library/Edward Baicy

Commander, U. S. Army Test and Evaluation Command

ATTN: DRSTE-FA/Mr. R. Gallasso

Commandant, U. S. Army Engineer School

ATTN: ATSEN-SY-L

Canadian Forces Liaison Officer, MERADCOM

ATTN: MAJ G. Focsaneanu

Commander, U. S. Army Engineer Division,

Huntsville

HNDED-CS/Michael M. Dembo ATTN:

Mr. Robert M. Wamsley

HNDED-CS/Mr. Paul LaHoud

HNDED-CS/Mr. Ron Lein

Commander, U. S. Army Engineer Division,

Middle East (REAR)

ATTN: A. Oliver Werner/MEDED-TS

Commander, U. S. Army Engineer District, Omaha

ATTN: Mr. Tim Knight

Mr. James L. Sack

Commander, U. S. Army Engineer Division,

Ohio River

ATTN: ORDAS-L/Technical Library

Director, U. S. Army Engineer Waterways

Experiment Station

5 cy ATTN: Library

DEPARTMENT OF THE ARMY (Continued)

Commander, U. S. Army Materials and Mechanics Research Center

ATTN: Technical Library

Commander, White Sands Missile Range ATTN: STEWS-TE-AN/Mr. Del La Paz

Commander, U. S. Army Tank-Automotive Research and Development Command ATTN: DRDTA-NR/Mr. R. Siorek

Commander, U. S. Army Materiel Development and Readiness Command (DARCOM)

ATTN: Technical Library

2 cy DRCRD-WN

Commander, U. S. Army Missile Command ATTN: Technical Library DRCPM-PE/William K. Jann

Commander, U. S. Army Mobility Equipment Research and Development Center ATTN: Technical Library

Commander, U. S. Army Nuclear and Chemical Agency
2 cy ATTN: Technical Library
MONA-WE
MONA-WE/COL Lowrey

Commander, U. S. Army Armament Command, Rock Island Arsenal ATTN: Technical Library

DEPARTMENT OF THE NAVY

Chief of Naval Operations, Department of the Navy ATTN: OP-985F

Officer-in-Charge, Civil Engineering Laboratory, Naval Construction Battalion Center ATTN: Mr. R. J. Odello W. A. Keenan R. Murtha

Technical Library

Commander, Naval Facilities Engineering Command

ATTN: Technical Library, Code 0911C

Superintendent, U. S. Naval Postgraduate School
ATTN: Library, Code 2124

Director, Naval Research Laboratory
ATTN: Code 2027, Technical Library

Commander, Naval Surface Weapons Center ATTN: Technical Library, Code X211 Code 1224, Navy Nuc Prgms Off

Commander, Naval Weapons Center ATTN: Code 533, Technical Library

Commander, Naval Weapons Evaluation Facility
ATTN: Technical Library

Chief of Naval Research
ATTN: Technical Library

DEPARTMENT OF THE NAVY (Continued)

Director, Strategic Systems Project Office ATTN: NSP-43, Technical Library

DEPARTMENT OF THE AIR FORCE

COL Joe Allen, AFOSR

Commander, Air Force Armament and Testing Laboratory, AFSC

ATTN: Technical Library
DLYV, G. R. Griner
DLYV, R. L. McGuire

AFESC/RDCS

ATTN: LT Tom Hilforty, WN Dr. Paul Thompson

Air Force Cambridge Research Laboratories, AFSC

ATTN: LwW, Dr. Ker Thompson SUOL AFCRL, Research Library

Air Force Institute of Technology ATTN: Technical Library

AFRCE-MX (DEEC)
ATTN: Mr. George Pace

U. S. Army Corps of Engineers, CEMXPA ATTN: ED-TS/Mr. Tash Tatsugawa MXPED-T/Mr. Robert Kelly

Commander, Ballistic Missile Office
ATTN: ENBF/LTC James N. McCallum
ENBF/LT Chris D. Ruff
ENSN/LT Dave Steinfield

Commander, Air Force Weapons Laboratory ATTN: DEV-S/Dr. T. Ross SUL, Technical Library NTE/Dr. M. A. Plamondon

Headquarters, Air Force Systems Command, Andrews Air Force Base ATTN: Technical Library

Commander, Armament Division
ATTN: DLODL/Technical Library

Commander, Foreign Technology Division, AFSC ATTN: TD-BTA Library Mr. Stan Spring

Commander, Rome Air Development Center, AFSC ATTN: EMTLD, Documents Library

Space and Missile Systems Organization ATTN: MMH/Hard Rock Silo Development MMH/Engineering Division

Commander, Strategic Air Command ATTN: NRI-STINFO Library

AF Office of Scientific Research ATTN: Jerry Bieleck

HQ SAC/XPFS

ATTN: MAJ K. L. Mills

APO and FPO

Landa Division, Infrastructure Branch ATTN: COL Jack Sullivan

USAFE EUROPE/DEXX

ATTN: MAJ H. Dean Bartel

DEPARTMENT OF DEFENSE CONTRACTORS

University of California ATTN: Joseph A. Smith/L-122

University of Florida ATTN: Dr. C. Allen Ross

University of Illinois
ATTN: Dr. J. D. Haltiwanger
Prof. A. H. S. Ang

University of Minnesota ATTN: Technical Library

University of New Mexico
ATTN: J. W. Jeter
H. L. Schreyer

Northwestern University
ATTN: Dr. Ted Belytchko

Aerospace Corporation
ATTN: Mr. Larry Selzer
Mr. Martin Eskijian
Mr. John Crawford

Agbabian Associates ATTN: Dr. M. S. Agbabian

Applied Research Inc. ATTN: Technical Library

Boeing Company ATTN: Mr. P. A. Krastins

California Research and Technology, Inc. ATTN: Marvin Ito Fred M. Sauer

Consulting and Special Engineering Services, Inc. ATTN: Dr. J. L. Merritt

Electromechanical Systems of New Mexico, Inc. ATTN: R. A. Shunk

DEPARTMENT OF DEFENSE CONTRACTORS (Continued)

General American Transportation Corp.
General American Research Division
ATTN: Library

IIT Research Institute
ATTN: Mr. A. Longinow

Institute for Defense Analyses
ATTN: IDA Librarian, Ruth S. Smith

Kaman Sciences Corporation
ATTN: Gunning Butler, Jr.

Mason & Hanger, Silas Mason Co., Inc. ATTN: A. T. Papp Larry L. Skeen

Physics International Company ATTN: Technical Library

R&D Associates

ATTN: Dr Harold L. Brode
Technical Library
Mr. J. G. Lewis

Science Applications, Inc.
ATTN: Dr. Michael D. McDonnell

Scientific Services, Inc.
ATTN: Dr. B. L. Gabrielsen

Southwest Research Institute ATTN: Mr. A. B. Wenzel Mr. Phil Nash

Stanford Research Institute
ATTN: Dr. G. Abrahamson
Jim Gran
Dr. A. Florence

Terra Tek, Inc. ATTN: Mr. S. J. Green

TRW Defense and Space Systems Group

ATTN: Dr. Richard Cramond

Mr. C. F. Buckey (523/300)

Technical Information Center/S-1930

Mr. Norman Lipner

Mr. Paul Chen

Weidlinger Associates, Consulting Engineers ATTN: Dr. Melvin L. Baron Dr. J. Isenberg

END

FILMED

2-85

DTIC